STRESS AND SHAPE ANALYSIS OF A PARAGLIDER WING

by

Robert W. Fralich

Thesis submitted to the Graduate Faculty of the

Virginia Polytechnic Institute

in candidacy for the degree of

DOCTOR OF PHILOSOPHY

in

ENGINEERING MECHANICS

June 1963

Blacksburg, Virginia

II. TABLE OF CONTENTS

TABLES

IV. SYMBOLS

A	constant $\left(= \dfrac{\sin \vartheta_L}{\frac{l_K}{l_L} - \cos \vartheta_L} \right)$
a	determinant of the metric of the coordinate system in the deformed surface
a_n	coefficient of power series
$a_{\alpha\beta}$	the first fundamental (metric) tensor of the coordinate system in the deformed surface
$a^{\alpha\beta}$	the conjugate of $a_{\alpha\beta}$
$\bar{a}_\alpha$	covariant base vector of the deformed coordinate system
$b_{\alpha\beta}$	the second fundamental tensor of the deformed surface
C	constant of integration
C_D	drag coefficient $\left(= \dfrac{D}{qS} \right)$
C_L	lift coefficient $\left(= \dfrac{L}{qS} \right)$
C_p	pressure coefficient $\left(= \dfrac{X}{q} \right)$
C'	boundary contour in deformed surface
$c_{\alpha\beta}$	covariant absolute permutation tensor of the deformed coordinate system $(= 0, \sqrt{a}$ or $-\sqrt{a}$ as $\alpha = \beta$, $\alpha\beta = 12$ or $\alpha\beta = 21$, respectively)

$c^{\alpha\beta}$	contravariant absolute permutation tensor of the deformed coordinate system ($= 0, \sqrt{\frac{1}{a}}$ or $-\sqrt{\frac{1}{a}}$ as $\alpha = \beta$, $\alpha\beta = 12$ or $\alpha\beta = 21$, respectively)
D	drag force on wing
D_p	drag force on payload
d	distance between ends of leading-edge and keel booms $\left(= l_K \sqrt{2 - 2 \cos \beta(\theta_L) \cos \delta(\theta_L)}\right)$
F_{Kx_0}, F_{Ky_0}, F_{Kz_0}	components of resultant force of sail on keel boom in x_0, y_0, z_0 directions, respectively
F_{Lx_0}, F_{Ly_0}, F_{Lz_0}	components of resultant force of sail on leading-edge boom in x_0, y_0, z_0 directions, respectively
$\bar{F}_K$	resultant force of sail on keel boom $(= \bar{i}F_{Kx_0} + \bar{j}F_{Ky_0} + \bar{k}F_{Kz_0})$
$\bar{F}_L$	Resultant force of sail on leading-edge boom $(= \bar{i}F_{Lx_0} + \bar{j}F_{Ly_0} + \bar{k}F_{Lz_0})$
$f(x,\theta)$	function defined in equation (90)
$g(\theta), h(\theta)$	arbitrary functions of integration
$g_{\alpha\beta}$	the first fundamental (metric)ttensor of the undeformed coordinate system
I_1, J_1, K_1	components of $(\bar{\tau}_1)_L$ in x_0, y_0, z_0 directions, respectively
I_2, J_2, K_2	components of $(\bar{\tau}_2)_L$ in x_0, y_0, z_0 directions, respectively
$\bar{i}$, $\bar{j}$, $\bar{k}$	unit vectors in x_0, y_0, z_0 directions, respectively
$(\bar{i}, \bar{v})$	angle between $\bar{i}$ and $\bar{v}$ unit vectors
K'	Gaussian curvature of deformed surface

L	lift force on wing
L_α	covariant components of $\bar{L}$ in the deformed coordinate system
$\bar{L}$	unit vector in the deformed surface, normal to the boundary contour C'
l_K	length of keel boom
l_L	length of leading-edge boom
l_α	physical components of $\bar{L}$ in the deformed coordinate system
N	the number of stations used in finite difference procedure
N_x, N_θ, $N_{x\theta}$	stress resultants (see fig. 4)
$(N_x)_T$, $(N_\theta)_T$, $(N_{x\theta})_T$	stress resultants at trailing edge of sail
$N^{\alpha\beta}$	index notation for stress resultants ($N^{11} = N_x$, $N^{22} = N_\theta$, $N^{12} = N_{x\theta}$)
n	station number used in finite difference procedure ($= 0, 1, 2, \ldots N$)
$n^{\alpha\beta}$	tensor of internal forces acting on a deformed element of the shell
P_L, P_S	boundary forces in the surface normal and tangential to the deformed contour per unit length of the deformed contour
q	dynamic pressure $\left(= \frac{1}{2}\rho V^2\right)$
$R(\theta)$	parameter proportional to principal radius of curvature $\left(= \frac{1}{x} R_2\right)$

R_2	principal radius of curvature of deformed surface of sail
S	total surface area of sail ($= l_K l_L \sin \theta_L$)
S_α	covariant components of $\bar{S}$ in deformed coordinate system
$\bar{S}$	unit vector tangent to deformed boundary contour
s_α	physical components of $\bar{S}$ in the deformed coordinate system
U_L, U_S	displacements in the surface normal and tangential to the deformed boundary contour
U_α	covariant components of displacement in the deformed coordinate system
V	free-stream velocity
V_α	physical components of displacement in deformed coordinate system
W	weight of payload
X^α, X	components of applied surface force tangential and normal to deformed surface, respectively
X	pressure on deflected sail
x, θ	coordinates in surface of sail
x_K	point of action of resultant force of sail on keel boom
x_L	point of action of resultant force of sail on leading-edge boom
x_T	value of x at trailing edge of sail $\left(= \dfrac{l_K A}{\sin \theta + A \cos \theta}\right)$

x_0, y_0, z_0	rectangular Cartesian coordinates in which x_0 is alined with airstream and $x_0 - z_0$ plane is in the vertical plane of symmetry of the paraglider wing
x_1, y_1, z_1	rectangular Cartesian coordinates in which x_1 is alined with keel boom and $x_1 - z_1$ plane is in the vertical plane of symmetry of the paraglider wing
x_{OK}, y_{OK}, z_{OK}	x_0, y_0, z_0 coordinates of location of resultant force of sail on keel boom
x_{OL}, y_{OL}, z_{OL}	x_0, y_0, z_0 coordinates of location of resultant force of sail on leading-edge boom
$\bar{x}_0$, $\bar{z}_0$	location of lift and drag forces on wing, respectively
α	angle of attack of keel
β, δ	coordinates that describe deflected shape of sail
β_N	value of β at station N $(=\beta(\theta_L))$
β_n	value of β at station n
$\beta(\theta_L)$	value of β at leading-edge boom
$\gamma_{\alpha\beta}$	Lagrangian strain tensor of deflected surface
δ_N	value of δ at station N $(= \delta(\theta_L))$
δ_n	value of δ at station n
$\delta(\theta_L)$	value of δ at leading-edge boom
ϵ	the angle through which the flow is deflected by the surface of the sail

$\Theta(\theta)$	function defined in equation (129)
θ_L	value of θ at leading-edge boom
θ_g	the angle of glide of paraglider wing
$\bar{\nu}$	the unit vector normal to the deflected surface
ξ^α	curvilinear coordinates in the deformed surface
ξ	dummy variable of integration
ρ	density of air
$\bar{\tau}_\alpha$	unit base vectors tangent to the deformed surface and tangent to the deformed coordinate curves in the surface
$(\bar{\tau}_\alpha)_K$	values of $\bar{\tau}_\alpha$ at keel boom
$(\bar{\tau}_\alpha)_L$	values of $\bar{\tau}_\alpha$ at leading-edge boom
$\left\{ \begin{matrix} \alpha \\ \beta\gamma \end{matrix} \right\}'$	Christoffel symbols of the second kind for the deformed coordinate system

Subscripts:

$\|\| \alpha$	denotes covariant differentiation with respect to ξ^α in the deformed coordinate system
$,\alpha$	denotes partial differentiation with respect to ξ^α in the deformed coordinate system

The generalized range and summation conventions of tensor calculus are used whereby a suffix used an odd number of times ranges over the coordinates and a suffix used an even number of times is to be summed over the coordinates. Greek suffixes are used for coordinates in the surface.

V. INTRODUCTION

Requirements for recovering rocket boosters and for landing space vehicles have led to a search for lifting devices which have a variety of attributes. Such a device should have a low-weight and a small exposed area for the launch phase. The accelerations and temperatures during the reentry phase must not be too high. In addition, the device should have the capability to perform a controlled glide to a predetermined site and to make a safe landing at a low subsonic speed.

One device which has many desirable features is the paraglider wing. (See ref. 1.) This wing, which has also been designated by various authors as a parawing, Rogallo wing, or flex wing; has the lightweight characteristics and packaging capabilities of the parachute. It consists of leading-edge booms and a keel boom joined together at the nose and a flexible sail whose surface carries the aerodynamic pressure loading. (See fig. 1.) The payload is suspended beneath the wing by cables (shroud lines). The booms are constructed so that they may be folded when the paraglider wing is packaged and so that they are sufficiently stiff after the wing is deployed. One possible method of construction is to make use of inflatable structural members while another possibility is to make use of a hinged mechanism and to "rigidize" its joints upon deployment. In some versions of the paraglider the booms are maintained a fixed distance apart by a spreader bar while on others they are held apart elastically by a spring mechanism located at the nose.

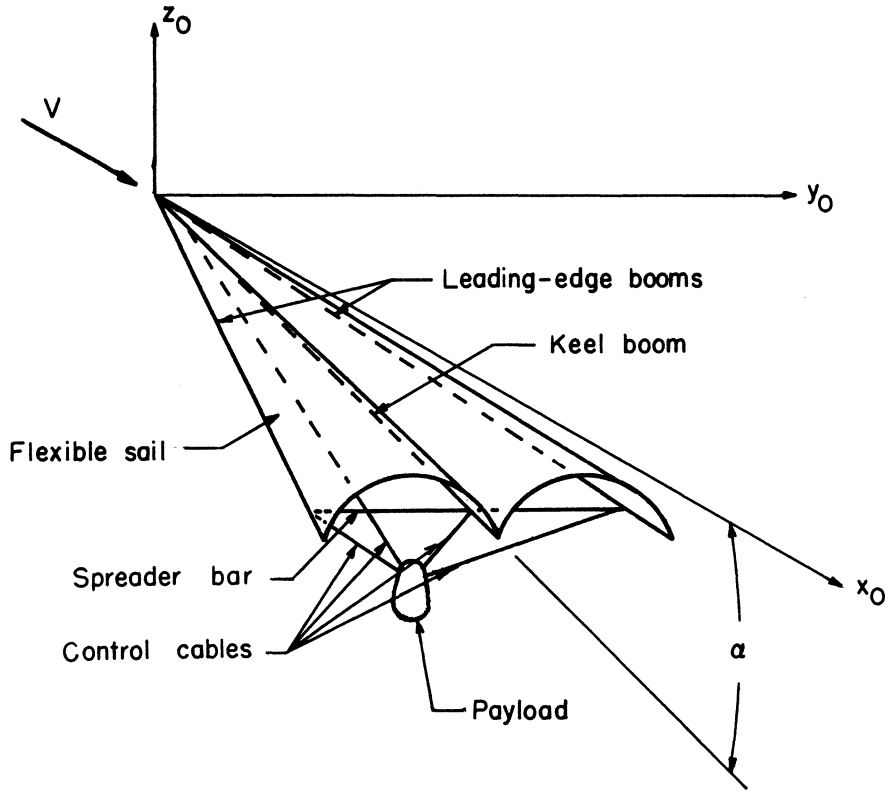

(a) Oblique view.

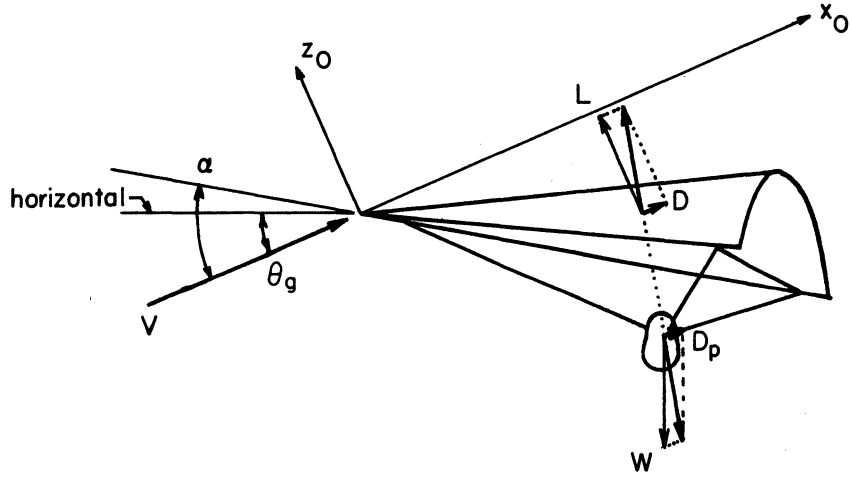

(b) Side elevation showing forces.

Figure 1.- Paraglider wing configuration.

The lightweight construction and packaging capabilities of the paraglider wing satisfy the requirements of lightweight and small exposed area for the launch phase. The wing can be deployed at the desired time for reentry and the glide back to earth. The preliminary calculations of reference 1 indicate that the accelerations can be held within desirable limits. The paraglider wing can be designed for very low wing loadings so that reentry temperatures may be kept from being prohibitive. Control of the glide is afforded by adjusting the length of the cables; this has the effect of positioning the payload with respect to the wing. (See fig. 1(b).) The wing then assumes an angle of attack α and glide angle θ_g such that the lift and drag forces, L and D, of the wing and the drag force, D_p, of the payload are in equilibrium with the weight W of the payload. In general the angle of attack is increased by moving the payload rearward and turns are executed by shifting the payload to the right or the left. The preliminary experimental investigation of reference 1 indicated that the paraglider can perform well at both subsonic and supersonic speeds. The current research effort is in the development of the paraglider for use at subsonic speeds in the termination of space flights. The immediate plans are to use the paraglider wing for the terminal recovery of the Gemini two-manned spacecraft. However, the paraglider is potentially useful for the whole mission from reentry flight at hypersonic speeds to the final low subsonic landing speed.

The previous investigations of paraglider wings have been mainly experimental in nature. The preliminary investigation of reference 1

consisted of wind-tunnel tests at subsonic and supersonic speeds and of free glide tests. In the wind-tunnel investigation of reference 2 the parawing was studied as an auxiliary low speed, high lift device on two supersonic airplane models. The free-flight investigation of reference 3 was concerned with the paraglider's stability and control. The supersonic wind-tunnel investigation reported in reference 4 was concerned with obtaining the lift and drag characteristics of the paraglider wing. Pressure distributions on three rigid wings, simulating paragliders, with varied canopy curvature and leading-edge sweep were obtained from wind-tunnel tests at subsonic and transonic speeds in references 5 and 6, respectively. In reference 7, the lift and drag coefficients were determined experimentally, at a Mach number of 6.6, for three rigid wings simulating paragliders with three canopy curvatures. These results were compared with theoretical results given by hypersonic Newtonian impact theory. In reference 8, full-scale wind-tunnel tests were performed to study the stability and control characteristics of a powered parawing airplane. The purpose of the investigations on the flexible paraglider wings was to find either the lift and drag characteristics or the stability and control characteristics. No attempt was made to find the deflected shape, the pressure distribution on the sail, or the stresses in the sail. Two of the investigations on the rigid idealizations (refs. 5 and 6) did yield pressure distributions. However, these pressure distributions apply to the fixed shape of the idealized wing and only represent the pressure distribution on the

flexible sail to an accuracy that depends on how well the rigid idealization represents the actual deflected shape of the flexible wing.

No previous theoretical investigations have been made on the flexible paraglider wing to obtain its shape and pressure distributions, the lift and drag coefficients, and the stresses in the sail. This situation is in part due to the complexity of the problem wherein the deflected shape of the sail depends on the pressure distribution over the surface of the sail and the pressure distribution in turn is aerodynamically dependent on the deflected shape of the sail. It is the purpose of this thesis to fill this gap in theoretical analysis.

The equilibrium equations for the sail are obtained by an application of the tensor equations of equilibrium derived in reference 9 for a nonlinear first approximation general shell and membrane theory. This nonlinear theory accounts for large deflections, large rotations and large strains. In applying the equilibrium equations to the flexible paraglider sail, the assumptions are made that the leading-edge and keel booms are rigid and straight and that the deformations of the sail are inextensional. The analysis is performed for a paraglider with the booms maintained a fixed distance apart by a spreader bar and with a trailing edge of the sail which is straight (when the sail is laid out in its flat condition). Other shapes of trailing edge can just as well be considered leading to different boundary conditions for the stress resultants at the trailing edge.

The equilibrium equations of the sail are solved explicitly for the stress resultants in terms of the pressure on the sail and a parameter that describes the shape of the sail. Then, equations are derived for the resultant forces applied by the sail to the keel and leading-edge booms and for the lift and drag coefficients. These equations for the resultant forces and the lift and drag coefficients are expressed in terms of the stress resultants in such a way that they may be used for any aerodynamic theory appropriate for the speed range under consideration. The boundary conditions on stress resultants at the trailing edge of the sail, after the adoption of an aerodynamic theory, yield a differential equation for obtaining the deflected shape of the sail. The equations are then specialized for Newtonian impact theory, which has sometimes been used to express the aerodynamic pressure-shape relationship for the hypersonic speed range. (See, for example, refs. 10 and 11.) This choice of aerodynamic theory is governed by two factors. First, Newtonian theory leads to a simplified analysis which shows the applicability of the present analysis in a simple manner. Second, this aerodynamic theory has been applied in reference 7 to a rigid idealization of a pareglider wing, and thus serves as a basis of comparison for the numerical results. Numerical results are obtained for a flexible configuration that corresponds to the rigid idealization in the sense that it has the same surface planform and the same keel and leading-edge locations. The variation of lift and drag coefficients with angle of attack are compared with those for the rigid idealization and the deflected

shape, pressure distribution and stress resultants in the sail are determined. Also, numerical results are presented to show effects of variation in dihedral angle (raising or lowering of the leading-edge booms).

VI. BASIC EQUATIONS FOR GENERAL MEMBRANE STRUCTURE

In the analysis of this thesis the tensor form of the equilibrium equations and boundary conditions derived in reference 9 are utilized. In this section a brief review is made of the basic tensor equations which are applicable to the analysis of the paraglider wing. The generalized range and summation conventions of tensor calculus are used whereby a suffix used an odd number of times ranges over the coordinates and a suffix used an even number of times is to be summed over the coordinates. Greek suffixes are used for coordinates in the surface.

A. Geometric Equations

The equilibrium equations are given in terms of coordinates ξ^α in the deformed equilibrium state. (See fig. 2.) The shape of the surface in this deformed state is defined by $a_{\alpha\beta}$, the first fundamental (metric) tensor, and $b_{\alpha\beta}$, the second fundamental tensor. Here

$$a_{\alpha\beta} = \bar{a}_\alpha \cdot \bar{a}_\beta \tag{1}$$

where $\bar{a}_\alpha$ are the covariant base vectors in the deformed surface and

$$b_{\alpha\beta} = -\bar{\nu} \cdot \bar{a}_{\alpha,\beta} = \bar{a}_\alpha \cdot \bar{\nu}_{,\beta} \tag{2}$$

where $\bar{\nu}$ is the unit outward normal to the deformed surface. The comma followed by the subscript β indicates partial differentiation with respect to ξ^β. The covariant base vectors $\bar{a}_\alpha$ are expressed

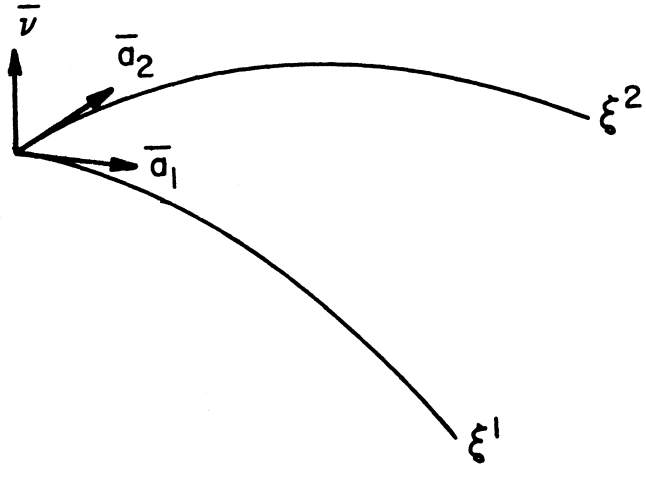

Figure 2.- Coordinates of deformed surface.

in terms of the unit tangential vectors $\bar{\tau}_\alpha$ in the deflected surface by the relations

$$\bar{\tau}_\alpha = \frac{1}{\sqrt{a_{\alpha\alpha}}} \bar{a}_\alpha \tag{3}$$

Some of the other relationships associated with the deformed surface are now reviewed. The conjugate metric tensor is given by the relationship

$$a^{\alpha\beta} = c^{\alpha\rho} c^{\beta\sigma} a_{\rho\sigma} \tag{4}$$

where $c^{\alpha\beta}$ is the (absolute) permutation tensor

$$\left.\begin{aligned} c^{\alpha\beta} &= 0 \quad \text{when} \quad \alpha = \beta \\ &= \frac{1}{\sqrt{a}} \quad \text{when} \quad \alpha\beta = 12 \\ &= -\frac{1}{\sqrt{a}} \quad \text{when} \quad \alpha\beta = 21 \end{aligned}\right\} \tag{5}$$

where the quantity a is the determinant of the metric tensor

$$a = a_{11} a_{22} - a_{12}^2 \tag{6}$$

The covariant permutation tensor is defined by

$$\left.\begin{aligned} c_{\alpha\beta} &= 0 \quad \text{when} \quad \alpha = \beta \\ &= \sqrt{a} \quad \text{when} \quad \alpha\beta = 12 \\ &= -\sqrt{a} \quad \text{when} \quad \alpha\beta = 21 \end{aligned}\right\} \tag{7}$$

The Codazzi equations for the deformed surface are given by

$$b_{\alpha 1}\|_2 - b_{\alpha 2}\|_1 = 0 \tag{8}$$

where the notation $||$ denotes covariant differentiation in the deformed coordinate system. The Gaussian curvature is given by

$$K' = \frac{1}{a}(b_{11}b_{22} - b_{12}^2) \tag{9}$$

and the strain tensor by

$$\gamma_{\alpha\beta} = \frac{1}{2}(a_{\alpha\beta} - g_{\alpha\beta}) \tag{10}$$

where $g_{\alpha\beta}$ is the first fundamental (metric) tensor of the undeformed surface.

B. Equilibrium Equations

The tensor form of the equilibrium equations are given by

$$\left.\begin{aligned} n^{\alpha\beta}{}_{||\alpha} + X^\beta &= 0 \\ -b_{\alpha\beta}n^{\alpha\beta} + X &= 0 \end{aligned}\right\} \tag{11}$$

Here $n^{\alpha\beta}$ is the symmetrized tensor of internal forces acting on a deformed element of the shell and X^β, X are tensor components of applied body forces in the surface and normal to the surface, respectively. Note that

$$n^{\alpha\beta}{}_{||\alpha} = n^{\alpha\beta}{}_{,\alpha} + \begin{Bmatrix} \alpha \\ \alpha\gamma \end{Bmatrix}' n^{\gamma\beta} + \begin{Bmatrix} \beta \\ \alpha\gamma \end{Bmatrix}' n^{\alpha\gamma} \tag{12}$$

where

$$\begin{Bmatrix} \beta \\ \alpha\gamma \end{Bmatrix}' = \frac{1}{2}\, a^{\beta\rho}(a_{\alpha\rho,\gamma} + a_{\gamma\rho,\alpha} - a_{\alpha\gamma,\rho}) \tag{13}$$

is the Christoffel symbol of the second kind for the deformed coordinate system.

C. Boundary Conditions

Boundary conditions along the boundary contour C' of the deformed surface are given by prescribing

$$P_L \text{ or } U_L$$
$$P_S \text{ or } U_S$$

where P_L and P_S are applied boundary forces per unit length in the surface normal and tangent to C', respectively, and U_L and U_S are the displacements of the boundary contour in the deformed surface away from its position in the undeformed surface normal and tangential to C', respectively. Here

$$\left.\begin{aligned} P_L &= L_\beta L_\alpha n^{\alpha\beta} \\ P_S &= S_\beta L_\alpha n^{\alpha\beta} \\ U_L &= L^\alpha U_\alpha \\ U_S &= S^\alpha U_\alpha \end{aligned}\right\} \tag{14}$$

where L_α and S_α are respectively the covariant components of the unit outward normal $\bar{L}$ and the unit tangent $\bar{S}$ to C' (in the direction of increasing S). The quantities L^α and S^α are the corresponding contravariant components. Since $\bar{L}$ and $\bar{S}$ are orthogonal vectors

$$\left.\begin{aligned} L_\alpha S^\alpha &= 0 \\ S_\alpha S^\alpha &= L_\alpha L^\alpha = 1 \end{aligned}\right\} \tag{15}$$

VII. ANALYSIS

A. Derivation of Equilibrium Equations for the Sail of the Paraglider

Consider the paraglider laid out on a plane and let the coordinates ξ^1 and ξ^2 be designated x and ϑ, respectively. (See fig. 3.) Since the paraglider wing is symmetric about the x_1 axis, and since only symmetric deformations are considered in the analysis, only that portion of the wing in the first quadrant need be considered. The keel is at $\vartheta = 0$ and the leading edge at $\vartheta = \vartheta_L$. It is assumed that the leading-edge booms, of length l_L, and the keel boom, of length l_K, are straight and rigid and that the sail is inextensible. It is also assumed that the trailing edge of the sail is straight and is expressed in terms of the rectangular Cartesian coordinates x_1, y_1 (fig. 3) by the equation

$$y_1 = A(l_K - x_1) \tag{16}$$

where

$$A = \frac{\sin \vartheta_L}{\frac{l_K}{l_L} - \cos \vartheta_L} \tag{17}$$

In terms of the coordinates x, ϑ the trailing edge of the sail is expressed by the equation

$$x_T = \frac{l_K A}{\sin \vartheta + A \cos \vartheta} \tag{18}$$

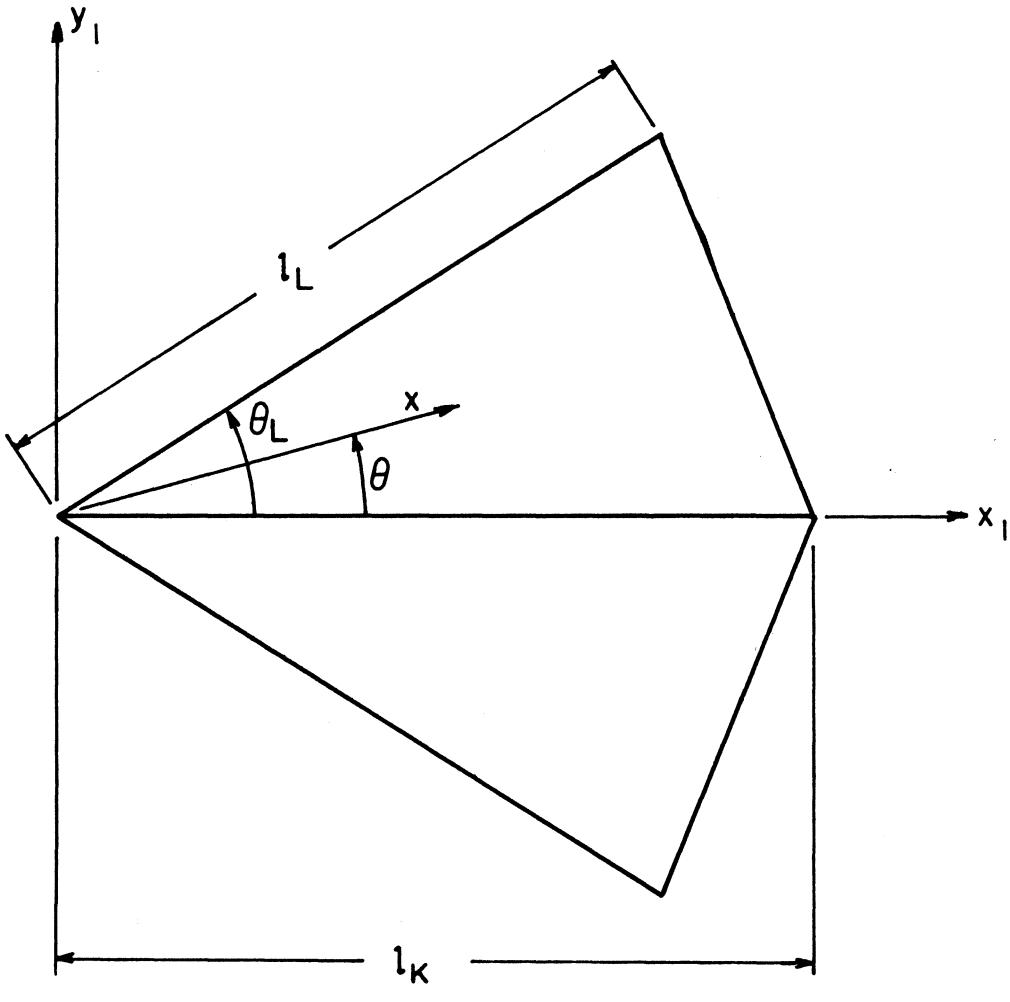

Figure 3.- Coordinates of sail.

Here a subscript T has been added to indicate that the values of x from this equation are values at the trailing edge.

Let the paraglider wing laid out in the plane position be the unloaded condition where the metric is $g_{\alpha\beta}$. Since the deformation of the sail is assumed inextensional the strain tensor vanishes; that is

$$\gamma_{\alpha\beta} = 0 \tag{19}$$

and therefore

$$a_{\alpha\beta} = g_{\alpha\beta} \tag{20}$$

Thus the coordinates in the surface remain undistorted.

For the x,θ coordinate system, the metric tensor is given by

$$a_{\alpha\beta} = \begin{bmatrix} 1 & 0 \\ 0 & x^2 \end{bmatrix} \tag{21}$$

the conjugate metric tensor by

$$a^{\alpha\beta} = \begin{bmatrix} 1 & 0 \\ 0 & \frac{1}{x^2} \end{bmatrix} \tag{22}$$

and the nonvanishing Christoffel symbols of the second kind by

$$\begin{Bmatrix} 1 \\ 22 \end{Bmatrix}' = -x$$

$$\begin{Bmatrix} 2 \\ 12 \end{Bmatrix}' = \begin{Bmatrix} 2 \\ 21 \end{Bmatrix}' = \frac{1}{x} \tag{23}$$

Since the x,θ coordinate curves are lines of principal curvature

$$b_{12} = b_{21} = 0 \tag{24}$$

Also since inextensional deformation of the sail is assumed, the surface is a developable surface for which the Gaussian curvature is zero. Thus upon substitution from equation (24) and equation (6) into equation (9), after use is made of equation (21)

$$K' = \frac{b_{11}b_{22}}{x^2} = 0 \tag{25}$$

Only the condition

$$b_{11} = 0 \tag{26}$$

yields a deflected shape of the sail for straight rigid booms. The only one of the Codazzi equations (8) not identically satisfied becomes

$$b_{21}\|_2 = b_{22}\|_1 \tag{27}$$

After covariant differentiation; equation (27) becomes

$$-\begin{Bmatrix} 2 \\ 12 \end{Bmatrix}' b_{22} = b_{22,1} - \begin{Bmatrix} 2 \\ 21 \end{Bmatrix}' b_{22} - \begin{Bmatrix} 2 \\ 1,2 \end{Bmatrix}' b_{22} \tag{28}$$

Substitution of the values of the Christoffel symbols from equations (23) gives the partial differential equation

$$\frac{\partial b_{22}}{\partial x} - \frac{1}{x} b_{22} = 0 \tag{29}$$

Solution of equation (29) yields

$$b_{22} = \frac{x}{R(\vartheta)} \tag{30}$$

where $R(\theta)$ is a function of θ alone. The radius of curvature R_2 is

$$R_2 = \frac{a_{22}}{b_{22}} \tag{31}$$

which upon substitution from equations (21) and (30) becomes

$$R_2 = xR(\theta) \tag{32}$$

The equilibrium equations (11), after substitution from equation (12), become

$$\left.\begin{aligned} &n^{\alpha\beta}{}_{,\alpha} + \begin{Bmatrix} \alpha \\ \alpha 1 \end{Bmatrix}' n^{1\beta} + \begin{Bmatrix} \alpha \\ \alpha 2 \end{Bmatrix}' n^{2\beta} + \begin{Bmatrix} \beta \\ \alpha 1 \end{Bmatrix}' n^{\alpha 1} + \begin{Bmatrix} \beta \\ \alpha 2 \end{Bmatrix}' n^{\alpha 2} + X^{\beta} = 0 \\ &-b_{22}n^{22} + X = 0 \end{aligned}\right\} \tag{33}$$

Upon substitution of expressions (23) for the Christoffel symbols and equation (30) for b_{22}, these equilibrium equations become

$$\left.\begin{aligned} &n^{11}{}_{,1} + n^{21}{}_{,2} + \frac{1}{x} n^{11} - xn^{22} = 0 \\ &n^{12}{}_{,1} + n^{22}{}_{,2} + \frac{3}{x} x^{12} = 0 \\ &n^{22} = \frac{RX}{x} \end{aligned}\right\} \tag{34}$$

In equations (34) the body forces X^1 and X^2 acting in the surface of the sail have been neglected as small compared to the normal pressure force X on the sail.

The equilibrium equations (34) are still in tensorial form and are now transformed into physical components. These transformations are given by the relations

$$\left.\begin{aligned} N_x &= \sqrt{\frac{a_{11}}{a^{11}}}\, n^{11} = n^{11} \\ N_\theta &= \sqrt{\frac{a_{22}}{a^{22}}}\, n^{22} = x^2 n^{22} \\ N_{x\theta} &= \sqrt{\frac{a_{22}}{a^{11}}}\, n^{12} = x n^{12} \end{aligned}\right\} \tag{35}$$

where N_x, N_θ, and $N_{x\theta}$ are the physical components of stress resultants. (See fig. 4.) Upon substitution of equation (35) the equilibrium equations (34) become

$$N_{x,x} + \frac{1}{x} N_{x\theta,\theta} + \frac{N_x - N_\theta}{x} = 0 \tag{36a}$$

$$\left(\frac{1}{x} N_{x\theta}\right)_{,x} + \frac{1}{x^2} N_{\theta,\theta} + \frac{3}{x^2} N_{x\theta} = 0 \tag{36b}$$

$$N_\theta = x(RX) \tag{36c}$$

B. Boundary Conditions for the Sail of the Paraglider

In this section the stress boundary conditions at the trailing edge and the nose and the displacement boundary conditions at the keel and leading edges are presented. Let the physical stress components N_x, N_θ, and $N_{x\theta}$ be redefined as N^{11}, N^{22}, and N^{12}, respectively. Then equations (35) can be written as

$$N^{\alpha\beta} = \sqrt{\frac{a_{\beta\beta}}{a^{\alpha\alpha}}}\, n^{\alpha\beta} \tag{37}$$

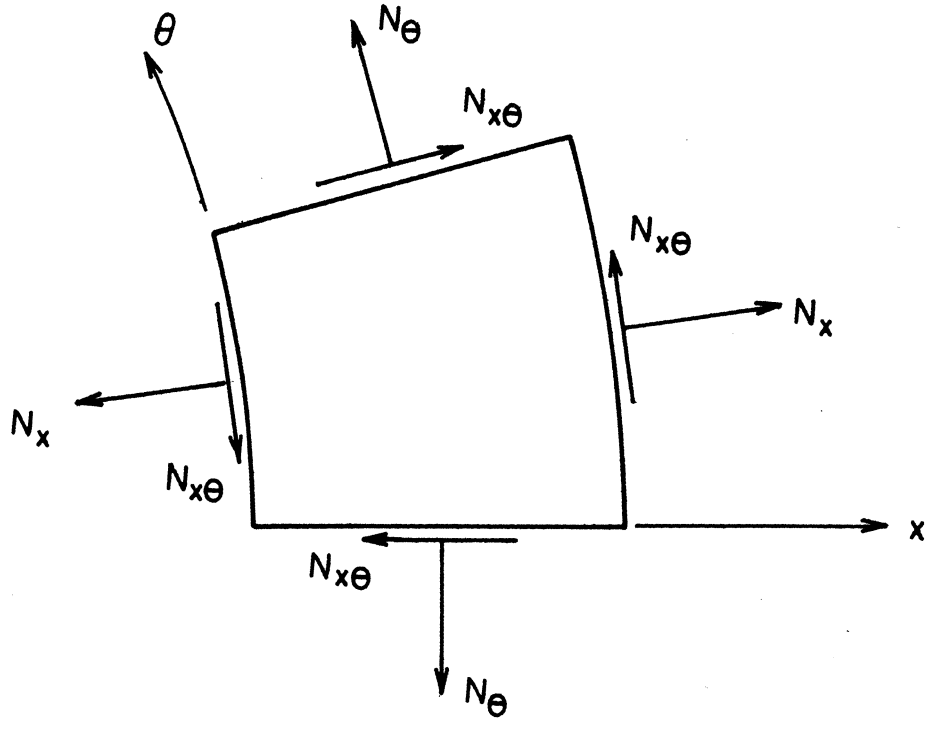

Figure 4.- Stress resultants on deflected surface of sail.

Let l_α, s_α be the physical components of the unit normal and tangent vectors to the boundary of the deflected sail. Then

$$l_\alpha = \frac{1}{\sqrt{a_{\alpha\alpha}}} L_\alpha = \frac{1}{\sqrt{a^{\alpha\alpha}}} L^\alpha \tag{38}$$

$$s_\alpha = \frac{1}{\sqrt{a_{\alpha\alpha}}} S_\alpha = \frac{1}{\sqrt{a^{\alpha\alpha}}} S^\alpha \tag{39}$$

Upon substitution of $n^{\alpha\beta}$, L_α, and S_α from equations (37), (38), and (39) into the first two of equations (14), then

$$\left.\begin{aligned} P_L &= l_\alpha l_\beta N^{\alpha\beta} \\ P_S &= s_\beta l_\gamma N^{\alpha\beta} \end{aligned}\right\} \tag{40}$$

Here P_L and P_S are physical forces per unit length.

The physical components of deflection are expressed by

$$V_\alpha = \frac{1}{\sqrt{a_{\alpha\alpha}}} U_\alpha \tag{41}$$

Upon substitution for U_α, L_α, and S_α from equations (41), (38), and (39), the last two of equations (14) yield

$$\left.\begin{aligned} U_L &= l_\alpha V_\alpha \\ U_S &= s_\alpha V_\alpha \end{aligned}\right\} \tag{42}$$

The quantities U_L and U_S are physical displacements of the boundary contour.

Substitution from equations (38) and (39) into equations (15) yields

$$s_1 l_1 + s_2 l_2 = 0 \tag{43}$$

$$s_1^2 + s_2^2 = 1 \tag{44}$$

$$l_1^2 + l_2^2 = 1 \tag{45}$$

From figure 5 it can be seen that

$$\left.\begin{aligned} s_1 &= \frac{dx}{ds} \\ s_2 &= x \frac{d\theta}{ds} \end{aligned}\right\} \tag{46}$$

For a given boundary contour, s_1 and s_2 can be found from equations (44) and (46) and l_1 and l_2 from equations (43) and (45). Then the boundary conditions for the given contour are determined from equations (40) or (42).

Trailing edge boundary conditions.- At the trailing edge the boundary contour is expressed by equation (18). From equations (18) and (46) the following is obtained:

$$(\sin \theta + A \cos \theta)s_1 + (\cos \theta - A \sin \theta)s_2 = 0 \tag{47}$$

Simultaneous solution of equations (44) and (47) yields

$$s_1 = -\frac{1}{\sqrt{1 + A^2}}(\cos \theta - A \sin \theta) \tag{48}$$

$$s_2 = \frac{1}{\sqrt{1 + A^2}}(\sin \theta + A \cos \theta) \tag{49}$$

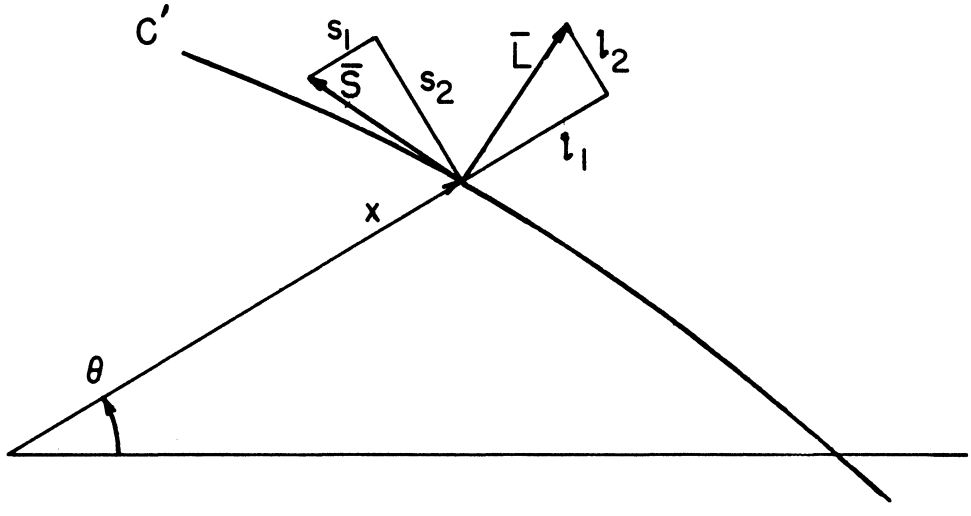

Figure 5.- Boundary vectors.

and the solution of equations (43) and (45) for l_1 and l_2 yields

$$l_1 = s_2 \tag{50}$$

$$l_2 = -s_1 \tag{51}$$

Now from equations (40), along the trailing edge

$$(P_L)_T = \frac{1}{1 + A^2}\Big[(\sin\theta + A\cos\theta)^2(N_x)_T + 2(\cos\theta - A\sin\theta)(\sin\theta + A\cos\theta)(N_{x\theta})_T + (\cos\theta - A\sin\theta)^2(N_\theta)_T\Big] = 0 \tag{52}$$

and

$$(P_S)_T = \frac{1}{1 + A^2}\Big[(\sin\theta + A\cos\theta)(\cos\theta - A\sin\theta)\big\{(N_\theta)_T - (N_x)_T\big\} + \big\{(\sin\theta + A\cos\theta)^2 - (\cos\theta - A\sin\theta)^2\big\}(N_{x\theta})_T\Big] = 0 \tag{53}$$

Solution of equation (52) for $(N_x)_T$ yields

$$(N_x)_T = -2\left(\frac{\cos\theta - A\sin\theta}{\sin\theta + A\cos\theta}\right)(N_{x\theta})_T - \left(\frac{\cos\theta - A\sin\theta}{\sin\theta + A\cos\theta}\right)^2(N_\theta)_T \tag{54}$$

which upon substitution into equation (53) yields

$$\Big[(\sin\theta + A\cos\theta)^2 + (\cos\theta - A\sin\theta)^2\Big]\Big[(N_{x\theta})_T + \left(\frac{\cos\theta - A\sin\theta}{\sin\theta + A\cos\theta}\right)(N_\theta)_T\Big] = 0 \tag{55}$$

Since

$$\left[(\sin\theta + A\cos\theta)^2 + (\cos\theta - A\sin\theta)^2\right] = 1 + A^2$$

can never vanish, equation (55) requires that

$$(N_{x\theta})_T = -\left(\frac{\cos\theta - A\sin\theta}{\sin\theta + A\cos\theta}\right)(N_\theta)_T \tag{56}$$

After substitution for $(N_{x\theta})_T$ from equation (56), equation (54) yields

$$(N_x)_T = \left(\frac{\cos\theta - A\sin\theta}{\sin\theta + A\cos\theta}\right)^2 (N_\theta)_T \tag{57}$$

Upon substitution from equations (18) and (36c) the boundary equations for stress at the trailing edge become

$$(N_{x\theta})_T = \left(\frac{dx_T}{d\theta}\right)(RX)_T \tag{58}$$

and

$$(N_x)_T = \frac{1}{x_T}\left(\frac{dx_T}{d\theta}\right)^2 (RX)_T \tag{59}$$

Keel boundary conditions.- Boundary conditions of zero displacement are specified at the keel. Now, along the keel

$$\left.\begin{aligned} l_1 &= 0 \\ l_2 &= -1 \\ s_1 &= 1 \\ s_2 &= 0 \end{aligned}\right\} \tag{60}$$

and the boundary conditions (42) become

$$\left.\begin{aligned} (U_L)_K &= -V_2 = 0 \\ (U_S)_K &= V_1 = 0 \end{aligned}\right\} \tag{61}$$

Leading-Edge Boundary Conditions.- At the leading edges the displacement is specified. Along this boundary

$$\left.\begin{aligned} t_1 &= 0 \\ t_2 &= 1 \\ s_1 &= -1 \\ s_2 &= 0 \end{aligned}\right\} \tag{62}$$

and the boundary equations (42) become

$$\left.\begin{aligned} (U_L)_L &= V_2 \\ (U_S)_L &= -V_1 \end{aligned}\right\} \tag{63}$$

Thus at the leading edge $(U_L)_L$ and $(U_S)_L$ have specified values.

Boundary conditions at the nose of the sail.- At the nose of the sail the stress resultants N_x, N_θ, and $N_{x\theta}$ must remain finite. These boundary conditions may be thought of as representing the limiting case for a stress-free boundary that shrinks to a point at the nose of the sail.

C. Representation of the Deflected Shape of Paraglider Sail

In the derivation of the equilibrium equations, the deflected shape of the sail has been represented by a parameter R which was shown to be proportional to the principal radius of curvature R_2 in equation (32). Also, in the boundary conditions at the keel and leading edges, the two deflection components V_1 and V_2 are specified. (See eqs. (61) and (63).) It is convenient in the

ensuing analysis to represent the deflected shape of the sail by the angles β and δ shown in figure 6. Here β and δ are functions of the coordinate θ and x,β,δ represent a set of spherical coordinates. The x_1-axis of the rectangular Cartesian coordinates x_1, y_1, z_1 is alined with the keel of the paraglider and the x_1z_1-plane is the vertical plane of symmetry of the paraglider. Hence

$$\left.\begin{aligned} z_1 &= x \sin \beta \\ x_1 &= x \cos \beta \cos \delta \\ y_1 &= x \cos \beta \sin \delta \end{aligned}\right\} \tag{64}$$

Consider the keel at an angle of attack α and define rectangular Cartesian coordinates x_0, y_0, z_0 such that the x_0-axis is alined with the direction of airflow. The x_0z_0-plane is coincident with the x_1z_1-plane (fig. 7), thus

$$\left.\begin{aligned} z_0 &= z_1 \cos \alpha - x_1 \sin \alpha \\ x_0 &= z_1 \sin \alpha + x_1 \cos \alpha \\ y_0 &= y_1 \end{aligned}\right\} \tag{65}$$

Upon substitution from equation (64) it can be shown that

$$\left.\begin{aligned} z_0 &= x(\sin \beta \cos \alpha - \cos \beta \cos \delta \sin \alpha) \\ x_0 &= x(\sin \beta \sin \alpha + \cos \beta \cos \delta \cos \alpha) \\ y_0 &= x \cos \beta \sin \delta \end{aligned}\right\} \tag{66}$$

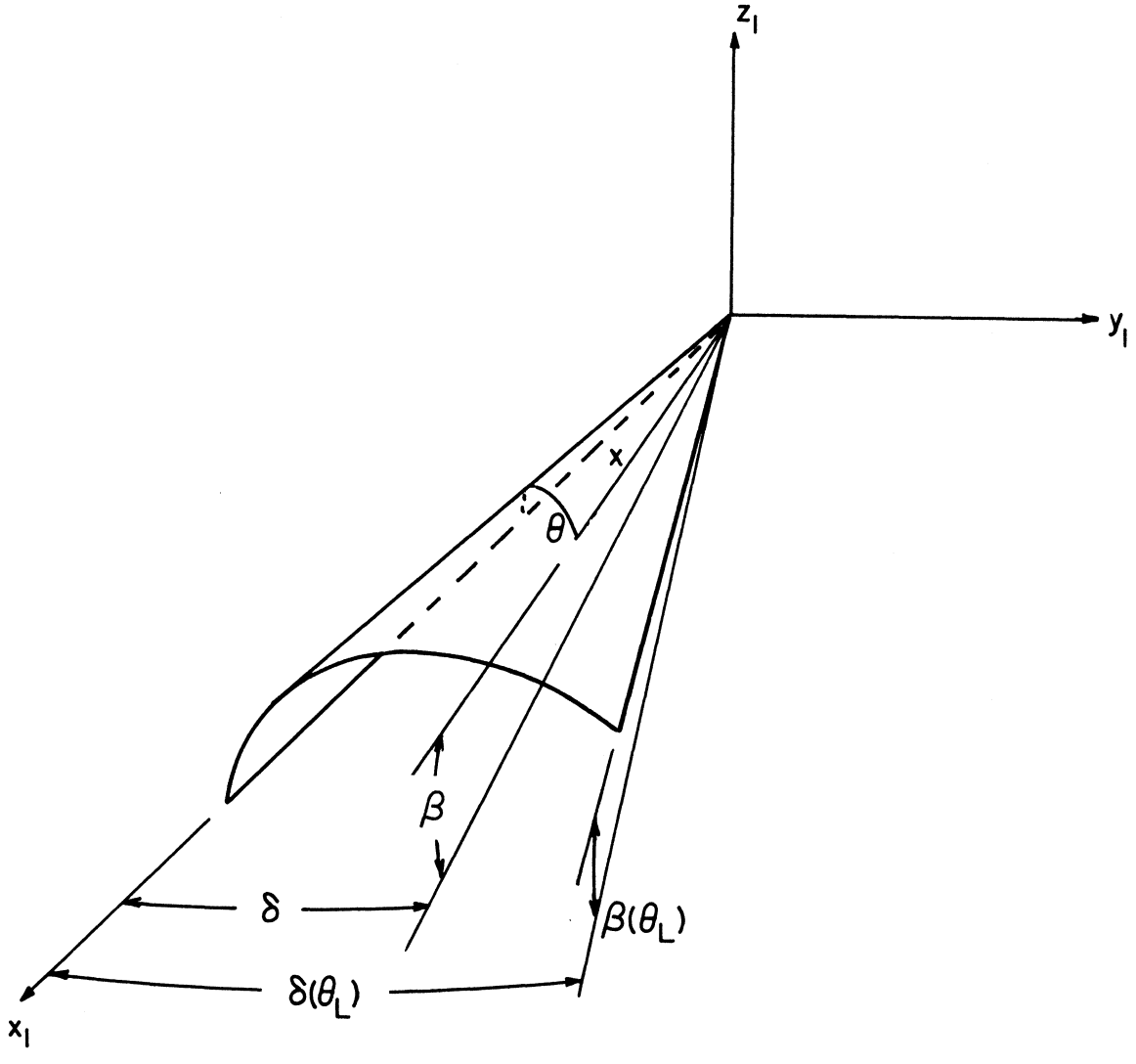

Figure 6.- Coordinates of deflected surface of sail.

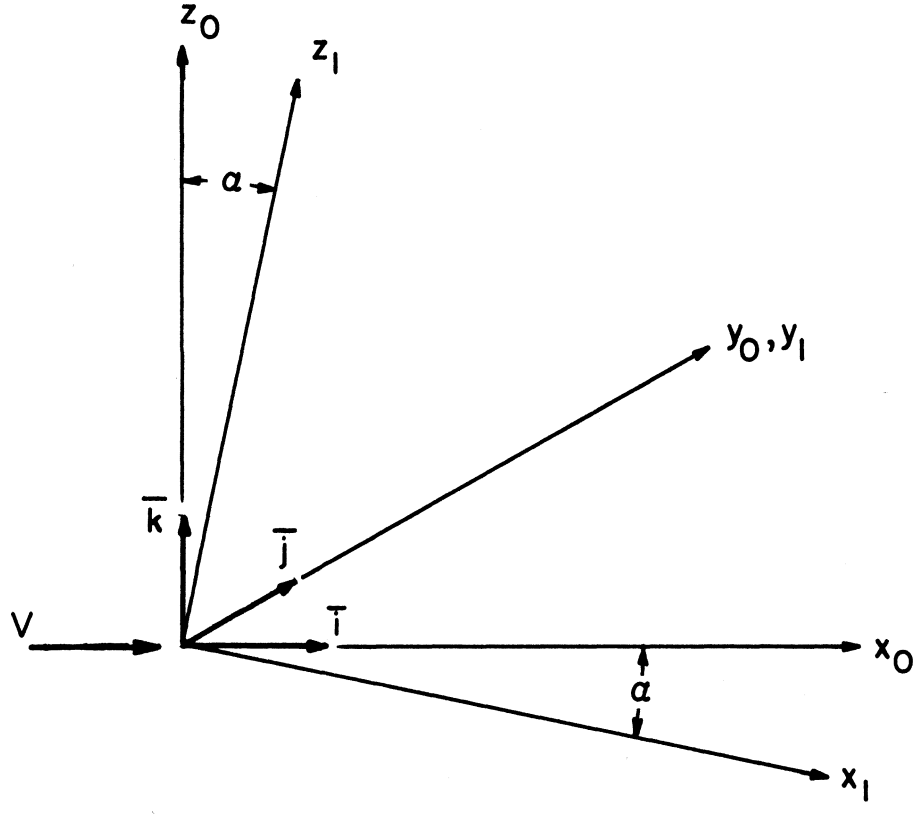

Figure 7.- Coordinate systems and unit vectors.

Now z_0 is treated as a function of x_0, y_0, that is, z_0 is the equation of the deflected surface in the x_0, y_0, z_0-coordinate system. Then

$$dz_0 = \frac{\partial z_0}{\partial x_0}\, dx_0 + \frac{\partial z_0}{\partial y_0}\, dy_0 \tag{67}$$

and from equations (66)

$$\left.\begin{aligned} dz_0 &= (\sin\beta\cos\alpha - \cos\beta\cos\delta\sin\alpha)dx \\ &\quad + x\left[(\cos\beta\cos\alpha + \sin\beta\cos\delta\sin\alpha)\frac{d\beta}{d\theta} + \cos\beta\sin\delta\sin\alpha\,\frac{d\delta}{d\theta}\right]d\theta \\ dx_0 &= (\sin\beta\sin\alpha + \cos\beta\cos\delta\cos\alpha)dx \\ &\quad + x\left[(\cos\beta\sin\alpha - \sin\beta\cos\delta\cos\alpha)\frac{d\beta}{d\theta} - \cos\beta\sin\delta\cos\alpha\,\frac{d\delta}{d\theta}\right]d\theta \\ dy_0 &= \cos\beta\sin\delta\,dx + x\left(-\sin\beta\sin\delta\,\frac{d\beta}{d\theta} + \cos\beta\cos\delta\,\frac{d\delta}{d\theta}\right)d\theta \end{aligned}\right\} \tag{68}$$

From equations (67) and (68) there results

$$\frac{\partial z_0}{\partial x_0} = \frac{-\sin\delta\cos\alpha\,\frac{d\beta}{d\theta} + (\sin\beta\cos\delta\cos\alpha - \cos\beta\sin\alpha)\cos\beta\,\frac{d\delta}{d\theta}}{-\sin\delta\sin\alpha\,\frac{d\beta}{d\theta} + (\sin\beta\cos\delta\sin\alpha + \cos\beta\cos\alpha)\cos\beta\,\frac{d\delta}{d\theta}} \tag{69}$$

and

$$\frac{\partial z_0}{\partial y_0} = \frac{\cos\delta\,\frac{d\beta}{d\theta} + \sin\beta\cos\beta\sin\delta\,\frac{d\delta}{d\theta}}{-\sin\delta\sin\alpha\,\frac{d\beta}{d\theta} + (\sin\beta\cos\delta\sin\alpha + \cos\beta\cos\alpha)\cos\beta\,\frac{d\delta}{d\theta}} \tag{70}$$

Also the square of the length of a line element on the surface is given by

$$ds^2 = dx_0^2 + dy_0^2 + dz_0^2 \tag{71}$$

which upon substitution from equations (68) yields

$$ds^2 = dx^2 + x^2\left[\left(\frac{d\beta}{d\theta}\right)^2 + \cos^2\beta\left(\frac{d\delta}{d\theta}\right)^2\right]d\theta^2 \tag{72}$$

However, from equation (21), the following relation must hold between β and δ:

$$\left(\frac{d\beta}{d\theta}\right)^2 + \cos^2\beta\left(\frac{d\delta}{d\theta}\right)^2 = 1 \tag{73}$$

This equation gives the condition for inextensional deformation of the sail when the deflections are represented by β and δ. Equation (73) upon solution for $\frac{d\delta}{d\theta}$ yields

$$\frac{d\delta}{d\theta} = \pm \frac{1}{\cos\beta}\sqrt{1 - \left(\frac{d\beta}{d\theta}\right)^2} \tag{74}$$

The unit outward normal to the deflected surface is given by

$$\bar{\nu} = \pm \frac{1}{\left[\left(\frac{\partial z_0}{\partial x_0}\right)^2 + \left(\frac{\partial z_0}{\partial y_0}\right)^2 + 1\right]^{1/2}}\left[-\frac{\partial z_0}{\partial x_0}\bar{i} - \frac{\partial z_0}{\partial y_0}\bar{j} + \bar{k}\right] \tag{75}$$

where the positive sign refers to surfaces which are concave downward, and the minus sign to those which are concave upward. The unit normals $\bar{i}$, $\bar{j}$, $\bar{k}$ are directed along the x_0, y_0, z_0-axes as shown in figure 7. Upon substitution from equations (69), (70), and (74) for $\frac{\partial z_0}{\partial x_0}$, $\frac{\partial z_0}{\partial y_0}$, and $\frac{d\delta}{d\theta}$ equation (75) yields

$$\bar{\nu} = \left[(\cos\beta \sin\alpha - \sin\beta \cos\delta \cos\alpha)\sqrt{1 - \left(\frac{d\beta}{d\theta}\right)^2} + \sin\delta \cos\alpha \frac{d\beta}{d\theta}\right]\bar{i}$$

$$- \left[\sin\beta \sin\delta \sqrt{1 - \left(\frac{d\beta}{d\theta}\right)^2} + \cos\delta \frac{d\beta}{d\theta}\right]\bar{j}$$

$$+ \left[(\cos\beta \cos\alpha + \sin\beta \cos\delta \sin\alpha)\sqrt{1 - \left(\frac{d\beta}{d\theta}\right)^2} - \sin\delta \sin\alpha \frac{d\beta}{d\theta}\right]\bar{k} \tag{76}$$

The unit tangential vector in the x-direction is given by

$$\bar{\tau}_1 = (\sin\beta \sin\alpha + \cos\beta \cos\delta \cos\alpha)\bar{i}$$

$$+ (\cos\beta \sin\delta)\bar{j} + (\sin\beta \cos\alpha - \cos\beta \cos\delta \sin\alpha)\bar{k} \tag{77}$$

and the unit tangential vector in the θ-direction by

$$\bar{\tau}_2 = \bar{\nu} \times \bar{\tau}_1$$

$$= \left[-\sin\delta \cos\alpha \sqrt{1 - \left(\frac{d\beta}{d\theta}\right)^2} + (\cos\beta \sin\alpha - \sin\beta \cos\delta \cos\alpha)\frac{d\beta}{d\theta}\right]\bar{i}$$

$$+ \left[\cos\delta \sqrt{1 - \left(\frac{d\beta}{d\theta}\right)^2} - \sin\beta \sin\delta \frac{d\beta}{d\theta}\right]\bar{j}$$

$$+ \left[\sin\delta \sin\alpha \sqrt{1 - \left(\frac{d\beta}{d\theta}\right)^2} + (\cos\beta \cos\alpha + \sin\beta \cos\delta \sin\alpha) \frac{d\beta}{d\theta}\right]\bar{k} \tag{78}$$

The covariant base vectors $\bar{a}_\alpha$ for the deflected surface are related to the unit tangential vectors by equation (3). Substitution from equations (21) into equation (3) yields

$$\begin{aligned} \bar{a}_1 &= \bar{\tau}_1 \\ \bar{a}_2 &= x\bar{\tau}_2 \end{aligned} \tag{79}$$

The quantity b_{22} is obtained in terms of the angle β by use of equation (2) with suffixes $\alpha = \beta = 2$. Thus

$$b_{22} = \bar{a}_2 \cdot \bar{\nu}_{,2} \tag{80}$$

which upon substitution from equations (76), (79), and (78) becomes

$$b_{22} = \frac{-x}{\sqrt{1 - \left(\frac{d\beta}{d\theta}\right)^2}} \left[\frac{\sin \beta}{\cos \beta} \left\{ 1 - \left(\frac{d\beta}{d\theta}\right)^2 \right\} + \frac{d^2\beta}{d\theta^2} \right] \tag{81}$$

Then from equation (30) the function $R(\theta)$ can be expressed in terms of the quantity β as follows:

$$R(\theta) = \frac{-\sqrt{1 - \left(\frac{d\beta}{d\theta}\right)^2}}{\frac{d^2\beta}{d\theta^2} + \frac{\sin \beta}{\cos \beta} \left\{ 1 - \left(\frac{d\beta}{d\theta}\right)^2 \right\}} \tag{82}$$

In summary, the deflected shape of the sail can be represented by the angles β and δ which are functions of the coordinate θ. (See fig. 6.) The quantity $R(\theta)$, which appears in the equilibrium equations (36) and in the trailing edge boundary conditions (58) and (59), is then related to β by equation (82). Furthermore, the keel boundary conditions (61) can be replaced by the boundary conditions

$$\left.\begin{aligned} \beta(0) &= 0 \\ \delta(0) &= 0 \end{aligned}\right\} \tag{83}$$

and the leading-edge boundary conditions (63) can be replaced by the specification of $\beta(\theta_L)$ and $\delta(\theta_L)$.

D. Solution of Equilibrium Equations

Substitution of the expression for N_θ from equation (36c) into equations (36a) and (36b) yields

$$(xN_x)_{,x} + N_{x\theta,\theta} = x(RX) \tag{84}$$

$$(x^2N_{x\theta})_{,x} = -x^2(RX)_{,\theta} \tag{85}$$

Integration of equation (85) yields

$$N_{x\theta} = \frac{1}{x^2}\left[-\int_0^x \xi^2(RX)_{,\theta}d\xi + g(\theta)\right] \tag{86}$$

where $g(\theta)$ is an arbitrary function of θ. Upon satisfying the boundary condition for finiteness of the stress resultant at the nose of the sail $(x = 0)$,

$$g(\theta) = 0 \tag{87}$$

so that

$$N_{x\theta} = -\frac{1}{x^2}\int_0^x \xi^2(RX)_{,\theta}d\xi \tag{88}$$

Substitution of $N_{x\theta}$ from equation (88) into equation (84) yields

$$(xN_x)_{,x} = f(x,\theta) \tag{89}$$

where

$$f(x,\theta) = x(RX) + \frac{1}{x^2}\int_0^x \xi^2(RX)_{,\theta\theta}d\xi \tag{90}$$

Equation (89), upon integration, gives

$$N_x = \frac{1}{x}\left[\int_0^x f(\xi,\theta)d\xi + h(\theta)\right] \tag{91}$$

where $h(\theta)$ is an arbitrary function of θ. Satisfying the boundary condition for finiteness of the stress resultant at $x = 0$ requires that

$$h(\theta) = 0 \tag{92}$$

Thus, upon using equation (90), equation (91) yields

$$N_x = \frac{1}{x}\int_0^x \left[\xi(RX) + \frac{1}{\xi^2}\int_0^\xi \lambda^2(RX)_{,\theta\theta}d\lambda\right]d\xi \tag{93}$$

After satisfying the boundary conditions (58) and (59) for stress resultants at the trailing edge of the sail, it is found that

$$(N_{x\theta})_T = -\frac{1}{x_T^2}\int_0^{x_T} \xi^2(RX)_{,\theta}d\xi = \frac{dx_T}{d\theta}(RX)_T \tag{94}$$

$$(N_x)_T = \frac{1}{x_T}\int_0^{x_T}\left[\xi(RX) + \frac{1}{\xi^2}\int_0^\xi \lambda^2(RX)_{,\theta\theta}d\lambda\right]d\xi = \frac{1}{x_T}\left(\frac{dx_T}{d\theta}\right)^2(RX)_T \tag{95}$$

Equations (94) and (95) determine the distribution of (RX) over the sail required to satisfy the stress resultant boundary conditions at the trailing edge of the sail.

It should be mentioned here that not all pressure distributions can satisfy the boundary conditions that the stress resultants

N_x, N_θ, and $N_{x\theta}$ remain finite at the nose of the sail. (See eqs. (88) and (93).) The pressure distribution cannot have a singularity at $x = 0$ which is stronger than $\frac{1}{x}$ as $x \to 0$. It is believed that most aerodynamic theories will satisfy this requirement.

E. Calculation of Lift and Drag Forces for the Paraglider Wing

In this section the lift and drag forces are derived. As a preliminary step, the resultant forces applied by the sail to the keel and leading-edge booms are obtained. These resultant forces and their locations are presented as these values are useful in obtaining the forces in the shroud lines and spreader bars of the paraglider.

The resultant force applied to the keel by the half of the sail considered in the analysis is obtained by integration of the stress resultants for the sail along the keel boundary. Thus the vector equation for the force is given by

$$\bar{F}_K = (\bar{\tau}_1)_K \int_0^{l_K} (N_{x\theta})_{\theta=0} dx + (\bar{\tau}_2)_K \int_0^{l_K} (N_\theta)_{\theta=0} dx \qquad (96)$$

and this force acts through the point $x = x_K$ of the keel, where

$$x_K = \frac{\int_0^{l_K} x(N_\theta)_{\theta=0} dx}{\int_0^{l} (N_\theta)_{\theta=0} dx} \qquad (97)$$

Here $(\bar{\tau}_1)_K$ and $(\bar{\tau}_2)_K$ are the unit tangent vectors of the surface at the keel. (Eqs. (77) and (78) evaluated at $\theta = 0$.) Thus

$$(\bar{\tau}_1)_K = \bar{i} \cos \alpha - \bar{k} \sin \alpha \tag{98}$$

$$(\bar{\tau}_2)_K = \bar{i} \sin \alpha \left(\frac{d\beta}{d\theta}\right)_{\theta=0} + \bar{j} \sqrt{1 - \left(\frac{d\beta}{d\theta}\right)^2_{\theta=0}} + \bar{k} \cos \alpha \left(\frac{d\beta}{d\theta}\right)_{\theta=0} \tag{99}$$

Similarly, the vector equation for resultant force applied by the sail to the leading-edge boom is given by

$$\bar{F}_L = -(\bar{\tau}_1)_L \int_0^{l_L} (N_{x\theta})_{\theta=\theta_L} dx - (\bar{\tau}_2)_L \int_0^{l_L} (N_\theta)_{\theta=\theta_L} dx \tag{100}$$

and this force acts through the point $x = x_L$ of the leading edge where

$$x_L = \frac{\int_0^{l_L} x(N_\theta)_{\theta=\theta_L} dx}{\int_0^{l_L} (N_\theta)_{\theta=\theta_L} dx} \tag{101}$$

In equation (100) $(\bar{\tau}_1)_L$ and $(\bar{\tau}_2)_L$ are the unit tangent vectors of the surface at the leading edge $\theta = \theta_L$. Thus from equations (77) and (78)

$$(\bar{\tau}_1)_L = \bar{i}I_1 + \bar{j}J_1 + \bar{k}K_1 \tag{102}$$

$$(\bar{\tau}_2)_L = \bar{i}I_2 + \bar{j}J_2 + \bar{k}K_2 \tag{103}$$

where

$$I_1 = \sin\beta(\theta_L)\sin\alpha + \cos\beta(\theta_L)\cos\delta(\theta_L)\cos\alpha \tag{104}$$

$$J_1 = \cos\beta(\theta_L)\sin\delta(\theta_L) \tag{105}$$

$$K_1 = \sin\beta(\theta_L)\cos\alpha - \cos\beta(\theta_L)\cos\delta(\theta_L)\sin\alpha \tag{106}$$

$$I_2 = -\sin\delta(\theta_L)\cos\alpha\sqrt{1 - \left(\frac{d\beta}{d\theta}\right)^2_{\theta=\theta_L}} + (\cos\beta(\theta_L)\sin\alpha - \sin\beta(\theta_L)\cos\delta(\theta_L)\cos\alpha)\left(\frac{d\beta}{d\theta}\right)_{\theta=\theta_L} \tag{107}$$

$$J_2 = \cos\delta(\theta_L)\sqrt{1 - \left(\frac{d\beta}{d\theta}\right)^2_{\theta=\theta_L}} - \sin\beta(\theta_L)\sin\delta(\theta_L)\left(\frac{d\beta}{d\theta}\right)_{\theta=\theta_L} \tag{108}$$

$$K_2 = \sin\delta(\theta_L)\sin\alpha\sqrt{1 - \left(\frac{d\beta}{d\theta}\right)^2_{\theta=\theta_L}} + (\cos\beta(\theta_L)\cos\alpha + \sin\beta(\theta_L)\cos\delta(\theta_L)\sin\alpha)\left(\frac{d\beta}{d\theta}\right)_{\theta=\theta_L} \tag{109}$$

The forces $\bar{F}_K$ and $\bar{F}_L$ can be expressed in components along the the x_0, y_0, z_0 axis as follows:

$$\bar{F}_K = \bar{i}F_{Kx_0} + \bar{j}F_{Ky_0} + \bar{k}F_{Kz_0} \tag{110}$$

$$\bar{F}_L = \bar{i}F_{Lx_0} + \bar{j}F_{Ly_0} + \bar{k}F_{Lz_0} \tag{111}$$

where

$$F_{Kx_0} = \cos\alpha \int_0^{l_K} (N_{x\theta})_{\theta=0} dx + \sin\alpha \left(\frac{d\beta}{d\theta}\right)_{\theta=0} \int_0^{l_K} (N_\theta)_{\theta=0} dx \tag{112}$$

$$F_{Ky_0} = \sqrt{1 - \left(\frac{d\beta}{d\theta}\right)^2_{\theta=0}} \int_0^{l_K} (N_\theta)_{\theta=0} dx \tag{113}$$

$$F_{Kz_0} = -\sin\alpha \int_0^{l_K} (N_{x\theta})_{\theta=0} dx + \cos\alpha \left(\frac{d\beta}{d\theta}\right)_{\theta=0} \int_0^{l_K} (N_\theta)_{\theta=0} dx \tag{114}$$

$$F_{Lx_0} = -I_1 \int_0^{l_L} (N_{x\theta})_{\theta=\theta_L} dx - I_2 \int_0^{l_L} (N_\theta)_{\theta=\theta_L} dx \tag{115}$$

$$F_{Ly_0} = -J_1 \int_0^{l_L} (N_{x\theta})_{\theta=\theta_L} dx - J_2 \int_0^{l_L} (N_\theta)_{\theta=\theta_L} dx \tag{116}$$

$$F_{Lz_0} = -K_1 \int_0^{l_L} (N_{x\theta})_{\theta=\theta_L} dx - K_2 \int_0^{l_L} (N_\theta)_{\theta=\theta_L} dx \tag{117}$$

The points x_K and x_L can be given in terms of the x_0, y_0, z_0 coordinates by equation (66); accordingly

$$x_{0K} = x_K \cos\alpha \tag{118}$$

$$y_{0K} = 0 \tag{119}$$

$$z_{OK} = -x_K \sin \alpha \tag{120}$$

$$x_{OL} = x_L I_1 \tag{121}$$

$$y_{OL} = x_L J_1 \tag{122}$$

$$z_{OL} = x_L K_1 \tag{123}$$

Finally when both halves of the symmetrical sail are considered (fig. 8), the lift and drag coefficients can be expressed as follows:

$$C_L = \frac{L}{qS}$$

$$= \frac{2}{qS}\left(F_{Kz_O} + F_{Lz_O}\right) \tag{124}$$

$$C_D = \frac{D}{qS}$$

$$= \frac{2}{qS}\left(F_{Kx_O} + F_{Lx_O}\right) \tag{125}$$

where L and D are the lift and drag forces, respectively, on the wing; $q = \frac{1}{2}\rho V^2$ is the dynamic pressure, and

$$S = l_K l_L \sin \vartheta_L \tag{126}$$

is the total surface area of the sail. The resultant of the lift and drag forces acts through the point $(\bar{x}_O, \bar{y}_O)$ where

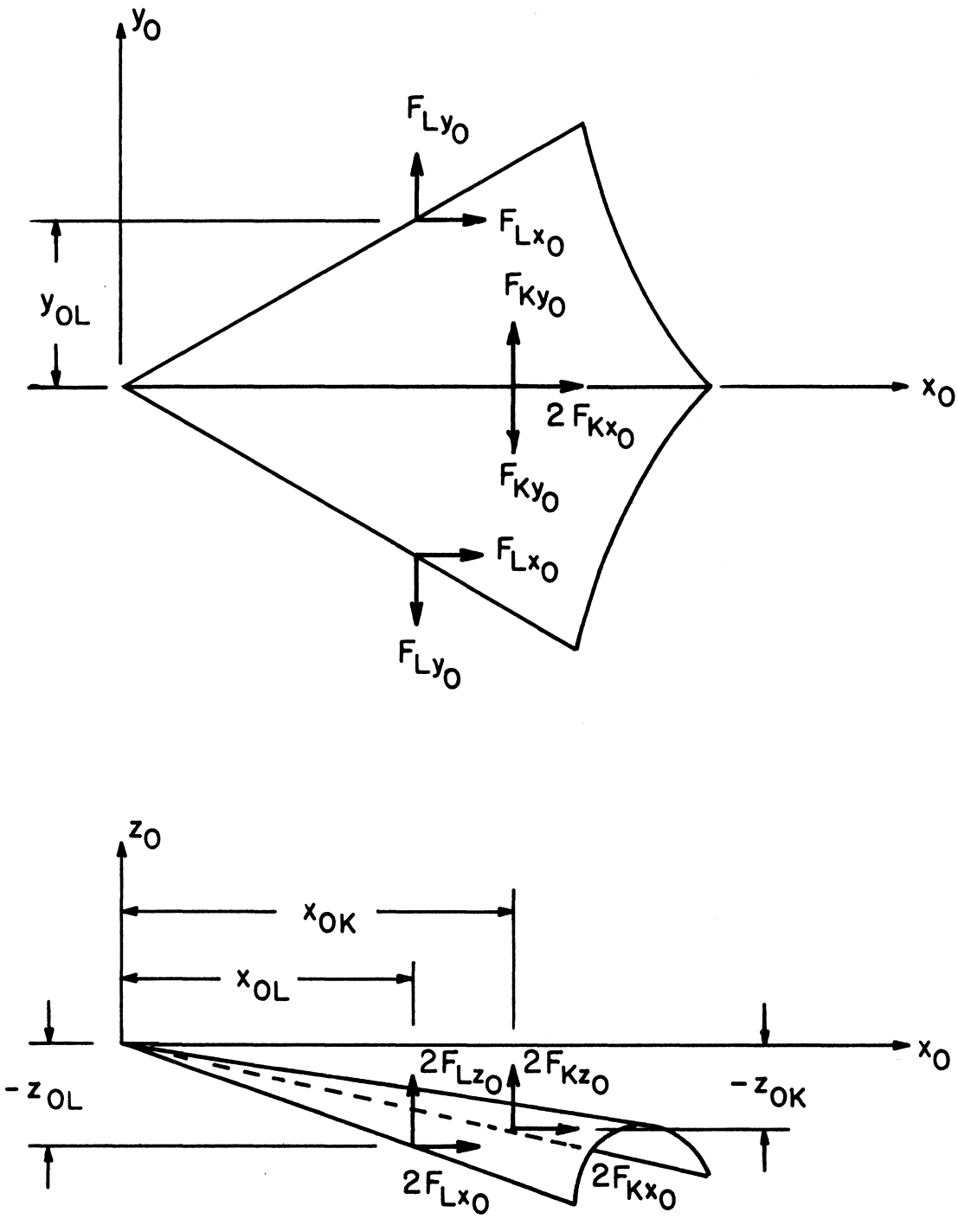

Figure 8.- Resultant forces applied by the sail to the keel and leading-edge booms.

$$\bar{x}_0 = \frac{x_{0L}F_{Lz_0} + x_{0K}F_{Kz_0}}{F_{Lz_0} + F_{Kz_0}} \tag{127}$$

and

$$\bar{z}_0 = \frac{z_{0L}F_{Lx_0} + z_{0K}F_{Kx_0}}{F_{Lx_0} + F_{Kx_0}} \tag{128}$$

F. Utilization of Aerodynamic Pressure-Deflected Shape Relationships

The entire analysis up to this point is based upon equilibrium considerations alone, and the equations derived are not dependent upon any specific aerodynamic theory. Although an aerodynamic pressure-deflected shape relationship is necessary, in order to determine the deflected shape of the sail, all of the previously derived equations are valid no matter which aerodynamic theory is used. Thus the analysis can be applied with the proper aerodynamic theory utilized for any speed range from hypersonic down through subsonic.

A brief review of the steps in the analysis is now in order. The stress resultants N_x, N_θ, and $N_{x\theta}$ have been expressed in terms of the normal pressure X and the shape of the sail given by R by means of equations (93), (36c), and (88). Furthermore, the distribution of the quantity (RX) over the sail, necessary to satisfy the boundary conditions on the stress resultants at the trailing edge of the sail, is governed by equations (94) and (95).

If the aerodynamic relation between the pressure and the deflected shape of the sail is utilized in equations (94) and (95), they provide the conditions for determining the deflected shape of the sail. Once the deflected shape that satisfies the boundary conditions at the keel and leading edge is known, the pressure X on the sail can be determined from the aerodynamic pressure-shape relationship. Then the stress resultants N_x, N_θ, and $N_{x\theta}$ can be determined by use of equations (36c), (88), and (93) along with equation (82). Finally, the resultant forces applied by the sail to the keel and leading-edge booms can be determined from equations (110) and (111) and the lift and drag coefficients can be determined from equations (124) and (125).

It is now of interest to consider the pressure distributions of some particular types of aerodynamic theories. For all aerodynamic theories that yield a pressure distribution X which satisfy the stress boundary conditions at the nose of the sail and for which separation of variables can be used equations (94) and (95) can be satisfied as follows: The most general such pressure distribution can be represented by

$$X = \Theta(\theta) \sum_{n=-1}^{\infty} a_n x^n \tag{129}$$

Then equation (94) upon integration over the variable θ yields

$$\int_0^{x_T} \xi^2 (RX) d\xi = \frac{C}{3} \tag{130}$$

where $\frac{C}{3}$ is a constant of integration. The distribution of (RX) over the surface of the sail, determined by equation (130) for pressure distributions of the type given in equation (129), also satisfies the condition given by equation (95). Thus equations (94) and (95) reduce to a single equation, equation (130). After use of an aerodynamic theory for the relationship between pressure and deflected shape, this equation becomes an ordinary differential equation for obtaining the parameter which defines the deflected shape. This analysis will be confined to consideration of aerodynamic theories which yield pressure distributions of this type. Introduction of theories of a more general type may require reexamination of the question of satisfaction of the boundary conditions at the trailing edge.

Aerodynamic theories that yield pressure distributions X which are independent of the x coordinate, lead to a still further simplification. For such theories, equation (130) becomes

$$(RX) = \frac{C}{x_T^3} \tag{131}$$

This equation, as for the case of equation (130), satisfies both of the trailing edge boundary conditions (94) and (95). The constant of integration C, is to be determined by the boundary conditions at the leading edge of the sail. With the relation (131) for (RX), the stress resultants from equations (36c), (93) and (88) become

$$
\left.
\begin{aligned}
N_\theta &= \frac{xC}{x_T^3} \\
&= \frac{xC}{l_K^3 A^3}(\sin\theta + A\cos\theta)^3 \\
N_x &= \frac{xC}{x_T^5}\left(\frac{dx_T}{d\theta}\right)^2 \\
&= \frac{xC}{l_K^3 A^3}(\sin\theta + A\cos\theta)(\cos\theta - A\sin\theta)^2 \\
N_{x\theta} &= \frac{xC}{x_T^4}\left(\frac{dx_T}{d\theta}\right) \\
&= -\frac{xC}{l_K^3 A^3}(\sin\theta + A\cos\theta)^2(\cos\theta - A\sin\theta)
\end{aligned}
\right\} \qquad (132)
$$

where A is given by equation (17).

Equation (131), after substitution of the aerodynamic pressure-deflected shape relations, represents the differential equation for determining the deflected shape.

VIII. APPLICATION OF NEWTONIAN IMPACT THEORY

A. Theory and Application to Paraglider Sail Analysis

In order to demonstrate an application of the analysis and to show numerical results, the method is used in conjunction with Newtonian impact theory. This theory, often used for hypersonic velocities, has the advantage of yielding pressures, X, which are functions of θ alone; thus, the simplified relations given in equations (131) and (132) can be used. In addition, this aerodynamic theory has also been applied in reference 7 to a rigid idealization of a paraglider wing, therefore, a direct comparison can be made between the actual flexible paraglider wing and its rigid counterpart.

In Newtonian impact theory the pressure coefficient, at a point, is given by the relation

$$\left.\begin{aligned} C_p &= 2 \sin^2\epsilon \quad \text{if} \quad \epsilon \geq 0 \\ C_p &= 0 \qquad\quad \text{if} \quad \epsilon < 0 \end{aligned}\right\} \qquad \text{or} \qquad (133)$$

where $C_p = \frac{X}{q}$. Here ϵ is the angle between the local streamwise unit tangent vector and the free-stream velocity vector. Newtonian impact theory requires that the moving stream give up its "normal" component of momentum (to the surface impacted); but it retains the tangential component which passes off tangentially to the local surface. Only portions of the surface that "see" the flow have a nonzero pressure coefficient, as indicated in equations (133).

If the free-stream velocity is along the x_0 axis, then from equation (76)

$$\cos(\bar{i},\bar{\nu}) = \bar{i} \cdot \bar{\nu} =$$

$$= (\cos\beta \sin\alpha - \sin\beta \cos\delta \cos\alpha)\sqrt{1 - \left(\frac{d\beta}{d\theta}\right)^2} + \sin\delta \cos\alpha \frac{d\beta}{d\theta} \tag{134}$$

where $(\bar{i},\bar{\nu})$ is the angle between the $\bar{i}$ and $\bar{\nu}$ unit vectors. From figure 9 which shows a trace of a plane passed through the $\bar{I}$ and $\bar{\nu}$ vectors

$$\cos(\bar{i},\bar{\nu}) = \cos\left(\frac{\pi}{2} - \epsilon\right) = \sin\epsilon \tag{135}$$

By use of equations (133), (134), and (135) the local pressure coefficient can be expressed as

$$C_p = 2\left[(\cos\beta \sin\alpha - \sin\beta \cos\delta \cos\alpha)\sqrt{1 - \left(\frac{d\beta}{d\theta}\right)^2} + \sin\delta \cos\alpha \frac{d\beta}{d\theta}\right]^2 \tag{136}$$

and the pressure on the sail at a given point is given by

$$X = 2q\left[(\cos\beta \sin\alpha - \sin\beta \cos\delta \cos\alpha)\sqrt{1 - \left(\frac{d\beta}{d\theta}\right)^2} + \sin\delta \cos\alpha \frac{d\beta}{d\theta}\right]^2 \tag{137}$$

The quantity δ, for the case of Newtonian impact theory, is given as follows by equation (74) where the positive sign is employed:

$$\delta = \int_0^\theta \frac{1}{\cos\beta}\sqrt{1 - \left(\frac{d\beta}{d\theta}\right)^2}\, d\theta \tag{138}$$

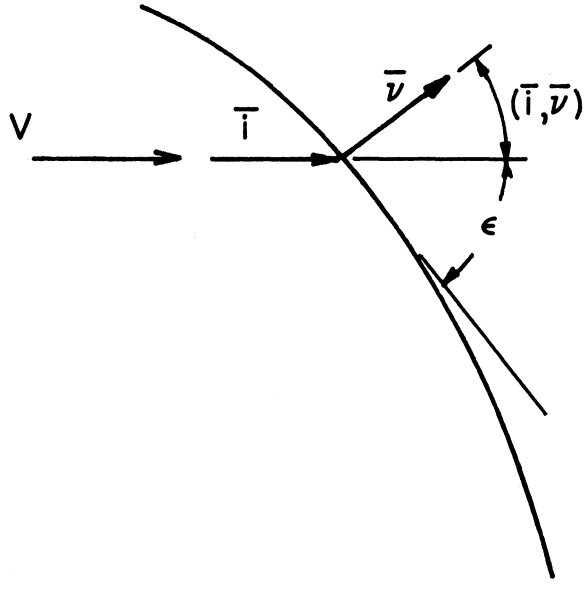

Figure 9.- Angle of deflection of air stream for Newtonian impact theory.

The negative sign for equation (74) is ruled out since the lower (or upstream) surface must "see" the flow at all times.

Equation (131), upon substitution from equation (137) for X and (82) for R, yields the differential equation by which the deflected shape of the sail is determined, thus

$$-\sqrt{1-\left(\frac{d\beta}{d\theta}\right)^2}\left[(\cos\beta\sin\alpha-\sin\beta\cos\delta\cos\alpha)\sqrt{1-\left(\frac{d\beta}{d\theta}\right)^2}\right.$$

$$\left.+\cos\alpha\sin\delta\frac{d\beta}{d\theta}\right]^2=\frac{1}{2}\left(\frac{C}{q l_K^3}\right)\left(\frac{1}{A}\sin\theta+\cos\theta\right)^3\left\{\frac{d^2\beta}{d\theta^2}+\frac{\sin\beta}{\cos\beta}\left[1-\left(\frac{d\beta}{d\theta}\right)^2\right]\right\} \tag{139}$$

Solution of the simultaneous nonlinear differential equations (138) and (139), for β and δ, and satisfying specified conditions $\beta(\theta_L)$ and $\delta(\theta_L)$, at the leading edge of the sail, determines the deflected shape of the sail.

The stress resultants N_θ, N_X, and $N_{X\theta}$ are obtained from equations (132). The components of resultant force applied to the keel and leading-edge booms are obtained from equations (112) through (117), after substitution from the last two of equations (132). In nondimensional form these resultant force components are

$$\frac{F_{Kx_0}}{qS}=-\frac{1}{2}\left(\frac{C}{q l_K^3}\right)\frac{l_K/l_L}{\sin\theta_L}\left[\frac{1}{A}\cos\alpha-\left(\frac{d\beta}{d\theta}\right)_{\theta=0}\sin\alpha\right] \tag{140}$$

$$\frac{F_{Ky_0}}{qS}=\frac{1}{2}\left(\frac{C}{q l_K^3}\right)\frac{l_K/l_L}{\sin\theta_L}\sqrt{1-\left(\frac{d\beta}{d\theta}\right)^2_{\theta=0}} \tag{141}$$

$$\frac{F_{Kz_0}}{qS} = \frac{1}{2}\left(\frac{C}{q l_3^3}\right)\frac{l_K/l_L}{\sin\theta_L}\left[\frac{1}{A}\sin\alpha + \left(\frac{d\beta}{d\theta}\right)_{\theta=0}\cos\alpha\right] \tag{142}$$

$$\frac{F_{Lx_0}}{qS} = \frac{1}{2}\left(\frac{C}{q l_K^3}\right)\frac{(l_K/l_L)^2}{\sin\theta_L}\left[I_1\,\frac{\cos\theta_L - l_L/l_K}{\sin\theta_L} - I_2\right] \tag{143}$$

$$\frac{F_{Ly_0}}{qS} = \frac{1}{2}\left(\frac{C}{q l_K^3}\right)\frac{(l_K/l_L)^2}{\sin\theta_L}\left[J_1\,\frac{\cos\theta_L - l_L/l_K}{\sin\theta_L} - J_2\right] \tag{144}$$

$$\frac{F_{Lz_0}}{qS} = \frac{1}{2}\left(\frac{C}{q l_K^3}\right)\frac{(l_K/l_L)^2}{\sin\theta_L}\left[K_1\,\frac{\cos\theta_L - l_L/l_K}{\sin\theta_L} - K_2\right] \tag{145}$$

where I_1, J_1, K_1, I_2, J_2, and K_2 are given by equations (104) through (109). The coordinates of the points through which these force components act are given by equations (118) through (123). Upon substitution from equations (97) and (101) these equations yield

$$x_{OK} = \frac{2}{3}\,l_K\cos\alpha \tag{146}$$

$$y_{OK} = 0 \tag{147}$$

$$z_{OK} = -\frac{2}{3}\,l_K\sin\alpha \tag{148}$$

$$x_{OL} = \frac{2}{3}\,l_L I_1 \tag{149}$$

$$y_{OL} = \frac{2}{3}\,l_L J_1 \tag{150}$$

$$z_{OL} = \frac{2}{3}\,l_L K_1 \tag{151}$$

The lift and drag coefficients, and the points through which the lift and drag forces act, are then determined by the use of equations (124), (125), (127), and (128).

B. Solution of Differential Equations for the Deflection of the Sail by Finite Differences

Equations (138) and (139) must be solved simultaneously for β and δ, and these quantities must satisfy the specified boundary conditions $\beta(\theta_L)$ and $\delta(\theta_L)$ at the leading edge of the sail. These equations are nonlinear and it is doubtful that a closed form solution could be found even for special cases. From the nature of the problem it is reasonable to assume that the sail would not have any unduly large curvatures; therefore, the derivatives of β with respect to θ can be represented by finite differences. Thus when the notation of figure 10 is used, the first and second derivatives at station n are given by

$$\left(\frac{d\beta}{d\theta}\right)_n = \frac{1}{2\Delta}(\beta_{n+1} - \beta_{n-1}) \tag{152}$$

and

$$\left(\frac{d^2\beta}{d\theta^2}\right)_n = \frac{1}{\Delta^2}(\beta_{n+1} - 2\beta_n + \beta_{n-1}) \tag{153}$$

Parabolic integration is employed to evaluate the integral in equation (138). Thus δ_n, at station n, can be given in terms of δ_{n-1}, at station $n-1$, by the equation

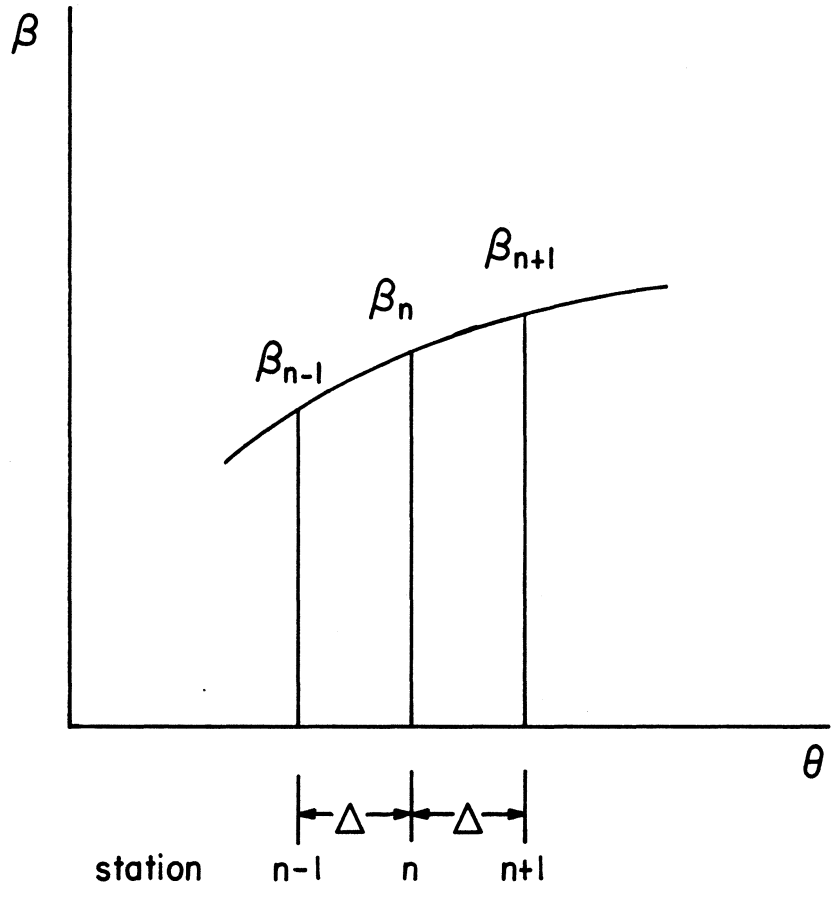

Figure 10.- Notations used for finite differences.

$$\delta_n = \delta_{n-1} + \int_{\theta_{n-1}}^{\theta_n} f(\theta)d\theta \tag{154}$$

where

$$f(\theta) = \frac{1}{\cos\beta}\sqrt{1 - \left(\frac{d\beta}{d\theta}\right)^2} \tag{155}$$

and

$$\int_{\theta_{n-1}}^{\theta_n} f(\theta)d\theta = \frac{\Delta}{12}\left[5f_n + 8f_{n-1} - f_{n-2}\right] \tag{156}$$

At station 0, located at the keel,

$$\beta_0 = \delta_0 = 0 \tag{157}$$

and equation (139), after application of equation (152) yields

$$\beta_1 = \Delta\left(\frac{d\beta}{d\theta}\right)_0 - \frac{\Delta^2\sin^2\alpha\left[1 - \left(\frac{d\beta}{d\theta}\right)_0^2\right]^{3/2}}{\frac{C}{qLK^3}} \tag{158}$$

where $\left(\frac{d\beta}{d\theta}\right)_0$ is the value of $\frac{d\beta}{d\theta}$ at the keel.

At station (1)

$$\delta_1 = \frac{\Delta}{12}\left[\frac{4}{\cos\beta_1}\sqrt{1 - \left(\frac{\beta_2}{2\Delta}\right)^2} + 8\sqrt{1 - \left(\frac{d\beta}{d\theta}\right)_0^2} - \frac{4}{\Delta}\frac{\left(\frac{d\beta}{d\theta}\right)_0\left\{\beta_1 - \Delta\left(\frac{d\beta}{d\theta}\right)_0\right\}}{\sqrt{1 - \left(\frac{d\beta}{d\theta}\right)_0^2}}\right] \tag{159}$$

and

$$-\sqrt{1-\left(\frac{\beta_2}{2\Delta}\right)^2}\left[(\cos\beta_1\sin\alpha-\sin\beta_1\cos\delta_1\cos\alpha)\sqrt{1-\left(\frac{\beta_2}{2\Delta}\right)^2}\right.$$

$$\left.+\sin\delta_1\cos\alpha\left(\frac{\beta_2}{2\Delta}\right)\right]^2=\frac{1}{2}\left(\frac{C}{qlK^3}\right)\left(\frac{1}{A}\sin\Delta+\cos\Delta\right)^3\left\{\frac{1}{\Delta^2}(\beta_2-2\beta_1)\right.$$

$$\left.+\frac{\sin\beta_1}{\cos\beta_1}\left[1-\left(\frac{\beta_2}{2\Delta}\right)^2\right]\right\} \qquad (160)$$

These two equations are to be solved simultaneously for β_2 and δ_1.

At station 2

$$\delta_2=\delta_1+\frac{\Delta}{12}\left[\frac{5}{\cos\beta_2}\sqrt{1-\left(\frac{\beta_3-\beta_1}{2\Delta}\right)^2}+\frac{8}{\cos\beta_1}\sqrt{1-\left(\frac{\beta_2}{2\Delta}\right)^2}-\sqrt{1-\left(\frac{d\beta}{d\theta}\right)_0^2}\right] \qquad (161)$$

and

$$-\sqrt{1-\left(\frac{\beta_3-\beta_1}{2\Delta}\right)^2}\left[(\cos\beta_2\sin\alpha-\sin\beta_2\cos\delta_2\cos\alpha)\sqrt{1-\left(\frac{\beta_3-\beta_1}{2\Delta}\right)^2}\right.$$

$$\left.+\sin\delta_2\cos\alpha\left(\frac{\beta_3-\beta_1}{2\Delta}\right)\right]^2=\frac{1}{2}\left(\frac{C}{qlK^3}\right)\left(\frac{1}{A}\sin2\Delta+\cos2\Delta\right)^3\left\{\frac{1}{\Delta^2}(\beta_3-2\beta_2+\beta_1)\right.$$

$$\left.+\frac{\sin\beta_2}{\cos\beta_2}\left[1-\left(\frac{\beta_3-\beta_1}{2\Delta}\right)^2\right]\right\} \qquad (162)$$

from which β_3 and δ_2 are to be determined.

At station n, where $n = 3,4,\ldots N-1$, and N is the last station (at the leading edge)

$$\delta_n = \delta_{n-1} + \frac{\Delta}{12}\left[\frac{5}{\cos\beta_n}\sqrt{1-\left(\frac{\beta_{n+1}-\beta_{n-1}}{2\Delta}\right)^2} + \frac{8}{\cos\beta_{n-1}}\sqrt{1-\left(\frac{\beta_n-\beta_{n-2}}{2\Delta}\right)^2} - \frac{1}{\cos\beta_{n-1}}\sqrt{1-\left(\frac{\beta_{n-1}-\beta_{n-3}}{2\Delta}\right)^2}\right] \tag{163}$$

and

$$-\sqrt{1-\left(\frac{\beta_{n+1}-\beta_{n-1}}{2\Delta}\right)^2}\left[(\cos\beta_n\sin\alpha - \sin\beta_n\cos\delta_n\cos\alpha)\sqrt{1-\left(\frac{\beta_{n+1}-\beta_{n-1}}{2\Delta}\right)^2} + \sin\delta_n\cos\alpha\left(\frac{\beta_{n+1}-\beta_{n-1}}{2\Delta}\right)\right]^2 = \frac{1}{2}\left(\frac{C}{q\ell K^3}\right)\left(\frac{1}{A}\sin n\Delta + \cos n\Delta\right)^3\left\{\frac{1}{\Delta^2}(\beta_{n+1} - 2\beta_n + \beta_{n-1}) + \frac{\sin\beta_n}{\cos\beta_n}\left[1-\left(\frac{\beta_{n+1}-\beta_{n-1}}{2\Delta}\right)^2\right]\right\} \tag{164}$$

From which β_{n+1} and δ_n are to be determined.

At station N

$$\delta_N = \delta_{N-1} + \frac{\Delta}{12}\left[\frac{5}{\cos\beta_N}\sqrt{1-\left(\frac{d\beta}{d\theta}\right)_N^2} + \frac{8}{\cos\beta_{N-1}}\sqrt{1-\left(\frac{\beta_N-\beta_{N-2}}{2\Delta}\right)^2} - \frac{1}{\cos\beta_{N-2}}\sqrt{1-\left(\frac{\beta_{N-1}-\beta_{N-3}}{2\Delta}\right)^2}\right] \tag{165}$$

and

$$-\sqrt{1-\left(\frac{d\beta}{d\theta}\right)_N^2}\left[(\cos\beta_N\sin\alpha - \sin\beta_N\cos\delta_N\cos\alpha)\sqrt{1-\left(\frac{d\beta}{d\theta}\right)_N^2} + \sin\delta_N\cos\alpha\left(\frac{d\beta}{d\theta}\right)_N\right]^2 = \frac{1}{2}\left(\frac{C}{q\ell K^3}\right)\left(\frac{1}{A}\sin N\Delta + \cos N\Delta\right)^3\left\{\frac{2}{\Delta}\left(\frac{d\beta}{d\theta}\right)_N - \frac{2}{\Delta^2}(\beta_N - \beta_{N-1}) + \frac{\sin\beta_N}{\cos\beta_N}\left[1-\left(\frac{d\beta}{d\theta}\right)_N^2\right]\right\} \tag{166}$$

from which $(d\beta/d\theta)_N$ and δ_N are to be determined.

If $(d\beta/d\theta)_0$, $(C/q l_K^3)$, and angle of attack α are known, then the step-by-step procedure indicated in equations (158) through (166) can be used to determine a possible deflected shape. For each set of values of $(d\beta/d\theta)_0$ and $(C/q l_K^3)$ chosen, at a given angle of attack, a set of values of $\beta_N = \beta(\theta_L)$ and $\delta_N = \delta(\theta_L)$ are obtained at the leading edge. The values of $(d\beta/d\theta)_0$ and $(C/q l_K^3)$ are then varied until the deflected shape, with the specified values of $\beta(\theta_L)$ and $\delta(\theta_L)$, is obtained. With $(d\beta/d\theta)_{\theta=0} = (d\beta/d\theta)_0$, $(d\beta/d\theta)_{\theta=\theta_L} = (d\beta/d\theta)_N$, $\beta(\theta_L) = \beta_N$, $\delta(\theta_L) = \delta_N$, and $(C/q l_K^3)$ known, the stress resultants N_θ, N_x, and $N_{x\theta}$ can be determined from equations (132). Then the resultant forces exerted by the sail on the keel and leading-edge booms can be determined from equations (140) through (151). Finally, the lift and drag coefficients and the location of the lift and drag forces can be determined from equations (124), (125), (127), and (128).

C. Numerical Results

In this section numerical results are presented for a configuration that corresponds in all possible respects to the rigid idealization analyzed in reference 7. This configuration has keel and leading-edge booms of equal length; and, in the undeflected flat condition, the angle θ_L (between the keel and leading-edge booms) is 45°. Boundary conditions which locate the leading-edge boom relative to the keel boom are chosen to correspond to one of the simulated canopy inflation conditions (180°) of the rigid idealization. These boundary conditions are given by

$$\left.\begin{aligned} \beta(\theta_L) &= 0 \\ \delta(\theta_L) &= 28.2^\circ \end{aligned}\right\} \tag{167}$$

which yields a distance between the ends of the leading-edge and keel booms equal to

$$\begin{aligned} d &= l_K \sqrt{2 - 2 \cos \beta(\theta_L) \cos \delta(\theta_L)} \\ &= 0.4872\ l_K \end{aligned} \tag{168}$$

The differential equation (139), for the deflected shape, and its auxiliary equation (138) were solved by the step-by-step procedure presented in equations (157) through (166). In these equations the finite differences were applied at intervals in θ of $\Delta = 1^\circ$. The problem was programed on the IBM 7090 digital computer, and deflected shapes were calculated for various angles of attack. From the calculated deflected shapes, the pressure coefficient, the stress resultants, the resultant forces applied by the sail to the keels, the lift and drag coefficients and the ratio of lift to drag were calculated for each angle of attack. These results of the calculations are given in table 1 and figures 11 through 15. The deflected shape of the surface of the sail is shown in figure 11 for angles of attack equal to 30°, 60°, and 90°. The variation of pressure coefficient over the surface of the sail, at these angles of attack are shown in figure 12. Since the constant of integration C is needed for calculating

TABLE 1. FORCE CHARACTERISTICS OF PARAGLIDER WING AT VARIOUS ANGLES OF ATTACK

α, deg	25	30	35	40	45	50	55
$(d\beta/d\theta)_0$	0.99895	0.99603	0.99234	0.98834	0.98433	0.9804	0.9767
C/ql_K^3	.004135	.01046	.01979	.03218	.04716	.06450	.08343
F_{Kx_0}/qS	.000137	.00103	.00322	.00724	.0134	.0221	.0332
F_{Ky_0}/qS	.000134	.000658	.00173	.00346	.00588	.00899	.0127
F_{Kz_0}/qS	.00516	.00791	.0147	.0233	.0330	.0432	.0531
F_{Lx_0}/qS	.000791	.00244	.00548	.0103	.0173	.0265	.0379
F_{Ly_0}/qS	-.00244	-.00578	-.0103	-.0159	-.0221	-.0289	-.0357
F_{Lz_0}/qS	.00185	.00497	.00967	.0157	.0227	.0300	.0369
x_{OK}/l_K	.604	.577	.546	.511	.471	.428	.382
y_{OK}/l_K	0	0	0	0	0	0	0
z_{OK}/l_K	-.282	-.333	-.382	-.428	-.471	-.511	-.546
x_{OL}/l_K	.533	.508	.481	.450	.415	.377	.336
y_{OL}/l_K	.315	.315	.315	.315	.315	.315	.315
z_{OL}/l_K	-.248	-.294	-.337	-.377	-.416	-.450	-.482
C_L	.0100	.0258	.0487	.0780	.111	.146	.180
C_D	.00185	.00695	.0174	.0351	.0615	.0973	.142
L/D	5.40	3.71	2.80	2.22	1.81	1.51	1.27
$\bar{x}_0/l_K$	.578	.551	.520	.486	.449	.408	.364
$\bar{z}_0/l_K$	-.253	-.306	-.354	-.398	-.440	-.478	-.512

TABLE 1. FORCE CHARACTERISTICS OF PARAGLIDER WING AT VARIOUS ANGLES OF ATTACK - Concluded

α, deg	60	65	70	75	80	85	90
$(d\beta/d\theta)_0$	0.9732	0.9698	0.9665	0.9639	0.9597	0.9562	0.9527
C/ql_K^3	.1035	.1243	.1445	.1648	.1832	.2003	.2145
F_{Kx_0}/qS	.0465	.0619	.0783	.0959	.113	.130	.144
F_{Ky_0}/qS	.0168	.0214	.0262	.0314	.0364	.0415	.0461
F_{Kz_0}/qS	.0619	.0690	.0735	.0757	.0744	.0702	.0628
F_{Lx_0}/qS	.0512	.0662	.0822	.0991	.115	.131	.144
F_{Ly_0}/qS	-.0426	-.0492	-.0550	-.0604	-.0648	-.0683	-.0703
F_{Lz_0}/qS	.0429	.0473	.0496	.0495	.0468	.0415	.0336
x_{OK}/l_K	.333	.282	.228	.172	.116	.0581	0
y_{OK}/l_K	0	0	0	0	0	0	0
z_{OK}/l_K	-.577	-.604	-.626	-.644	-.656	-.664	-.667
x_{OL}/l_K	.293	.248	.200	.151	.102	.0514	0
y_{OL}/l_K	.315	.315	.315	.315	.315	.315	.315
z_{OL}/l_K	-.509	-.532	-.552	-.568	-.579	-.585	-.587
C_L	.209	.233	.246	.250	.242	.223	.193
C_D	.195	.256	.321	.390	.457	.521	.578
L/D	1.07	.908	.767	.642	.531	.429	.334
$\ddot{x}_0/l_K$	.317	.268	.217	.164	.110	.0556	0
$\ddot{z}_0/l_K$	-.542	-.567	-.589	-.605	-.617	-.624	-.627

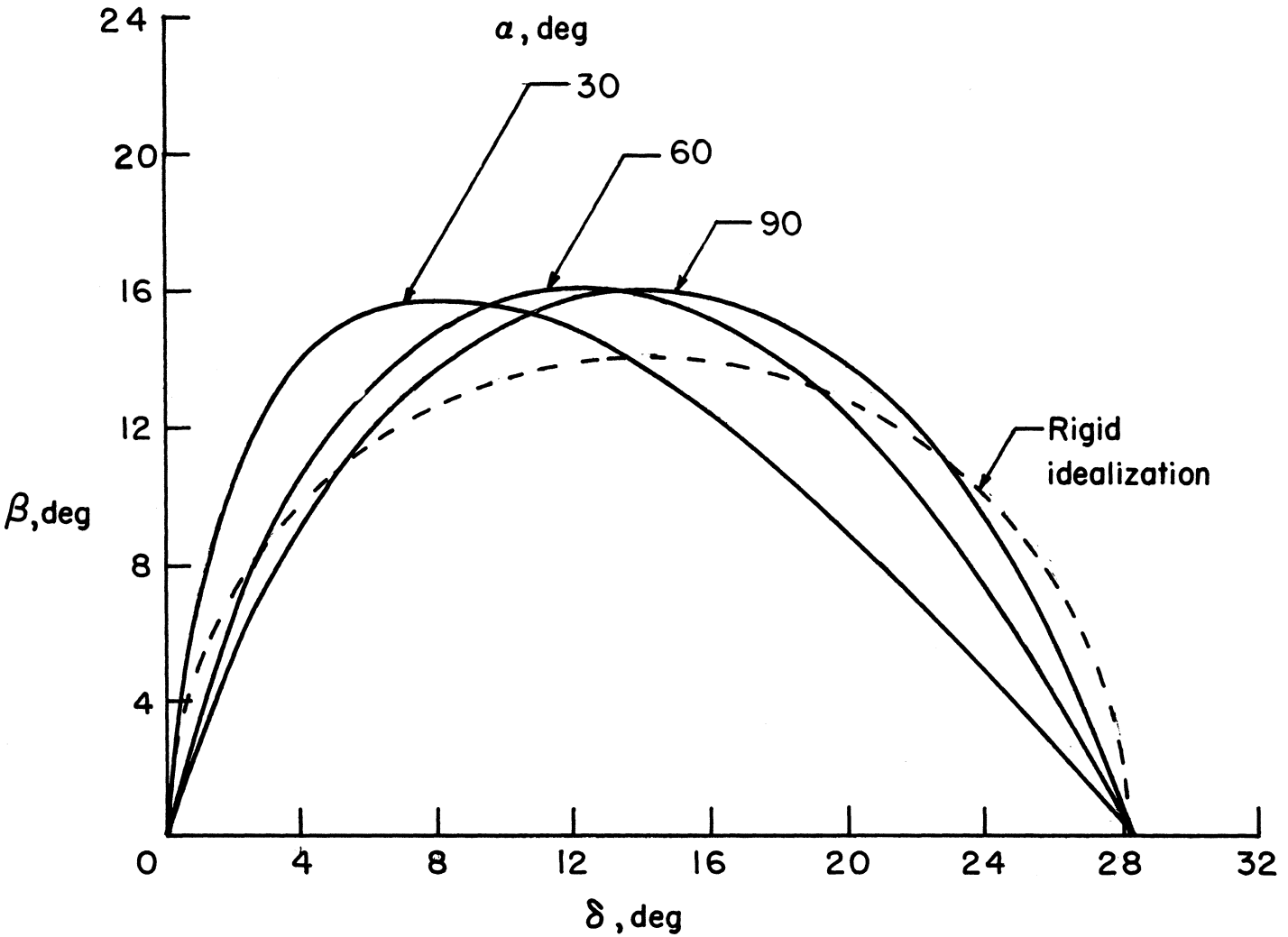

Figure 11.- Variation of deflected shape of surface with angle of attack.

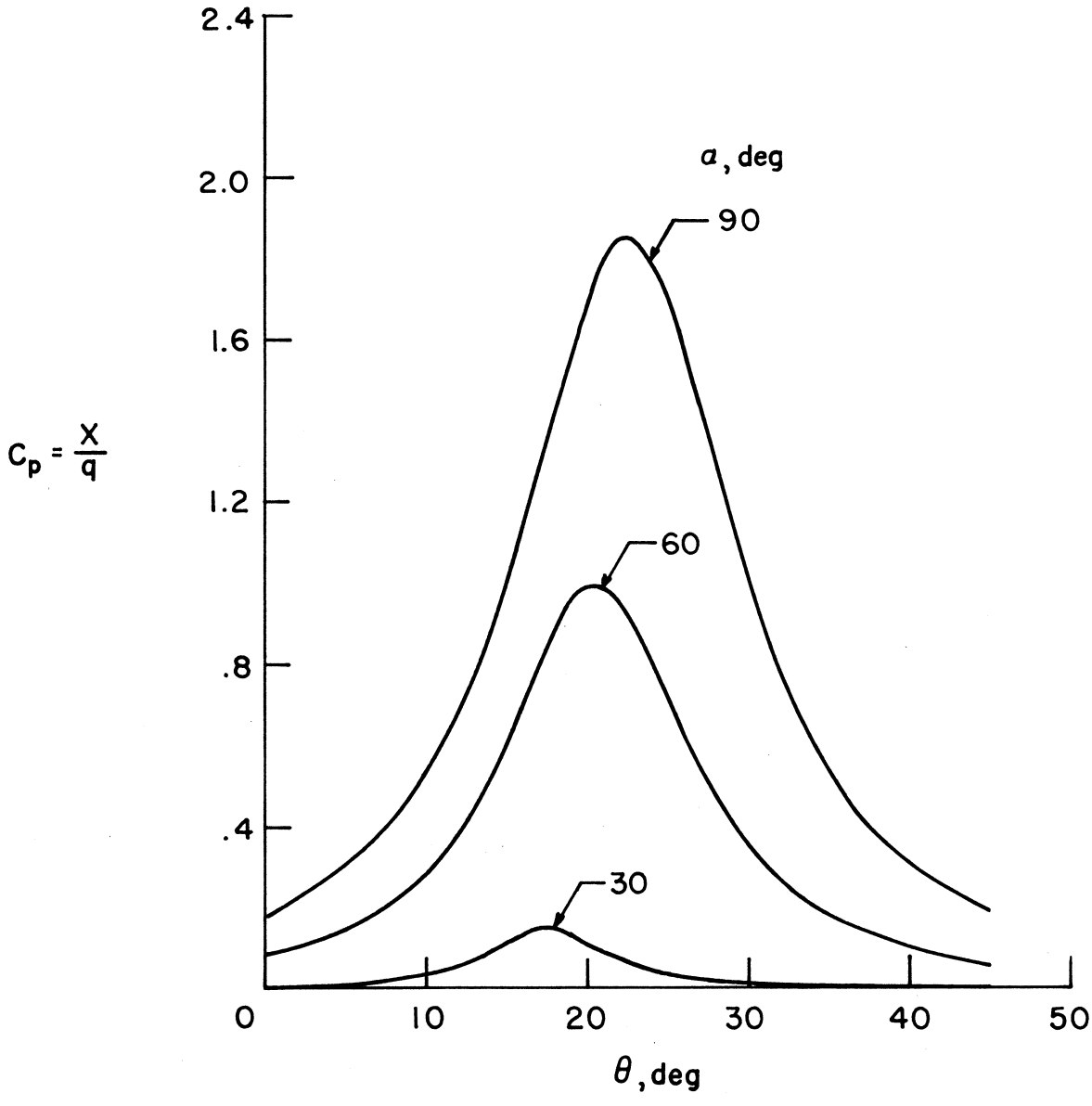

Figure 12.- Variation of pressure coefficient with angle of attack.

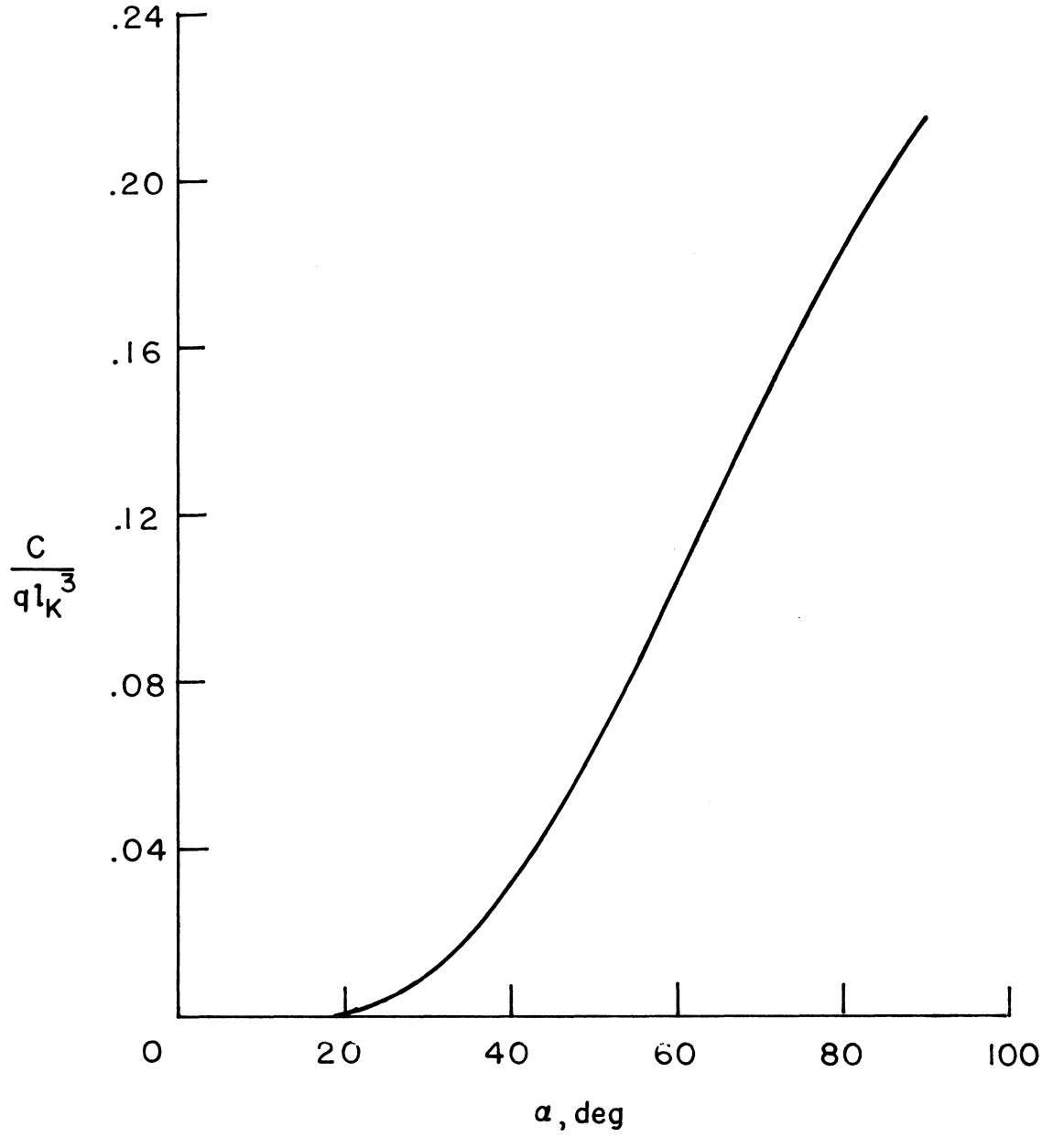

Figure 13.- Variation of C/ql_K^3 with angle of attack.

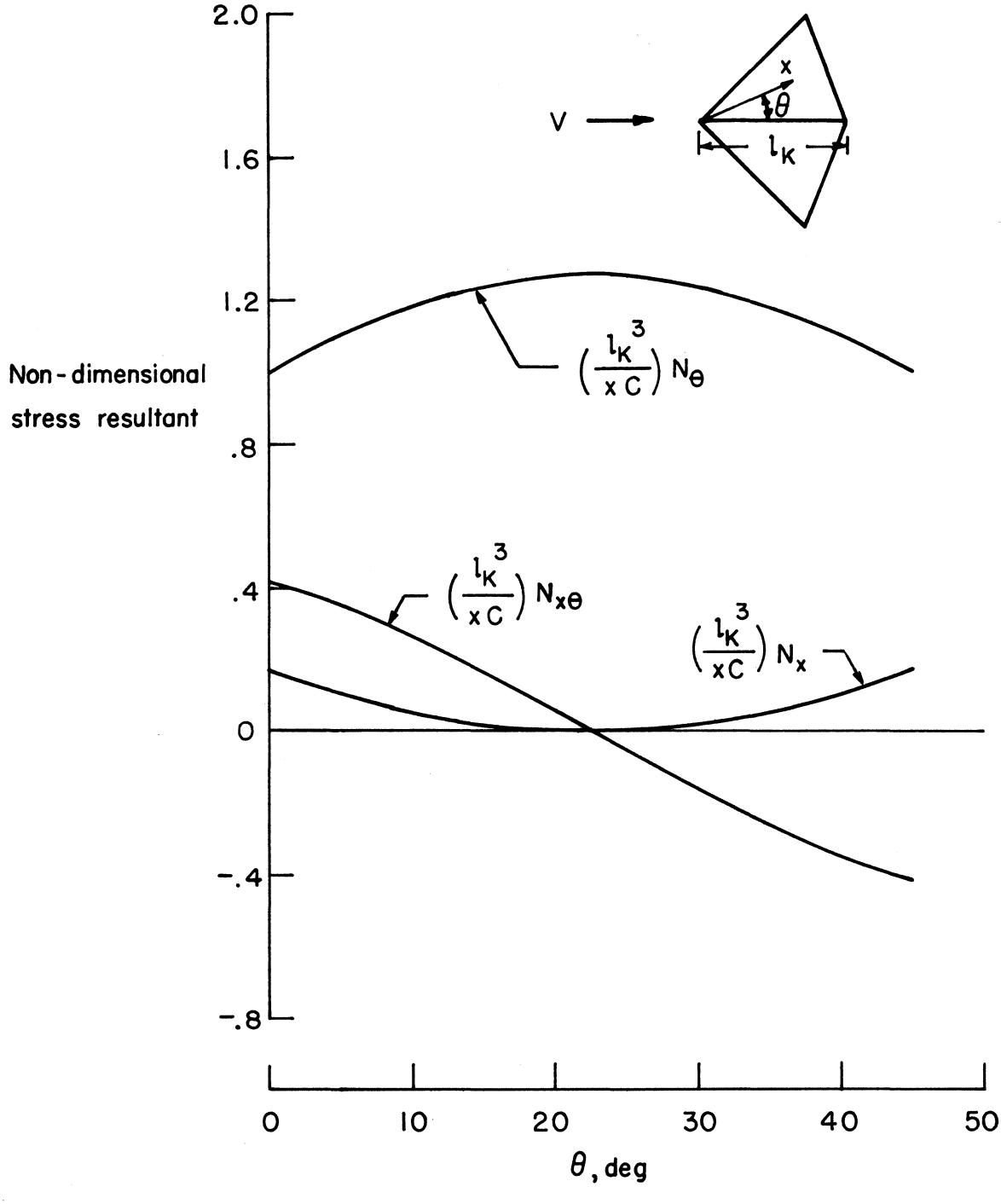

Figure 14.- Variation of stress resultants over surface of sail.

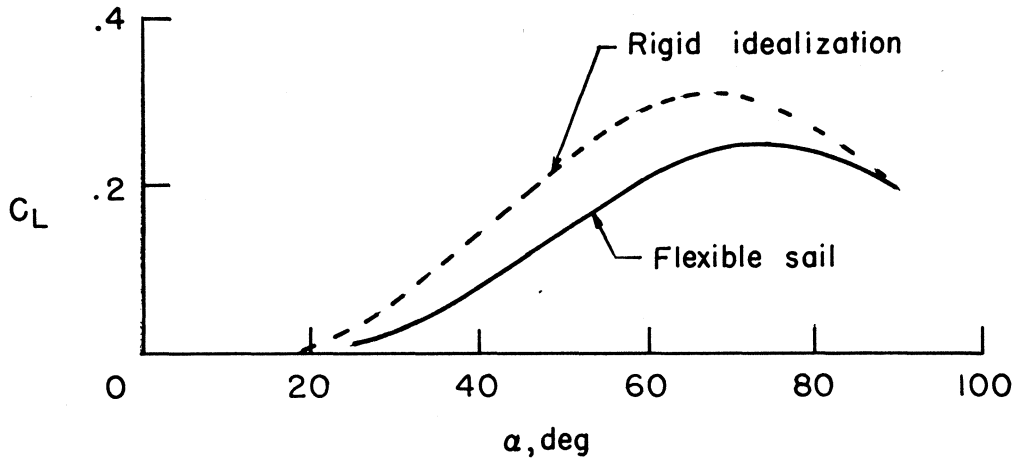

(a) Lift.

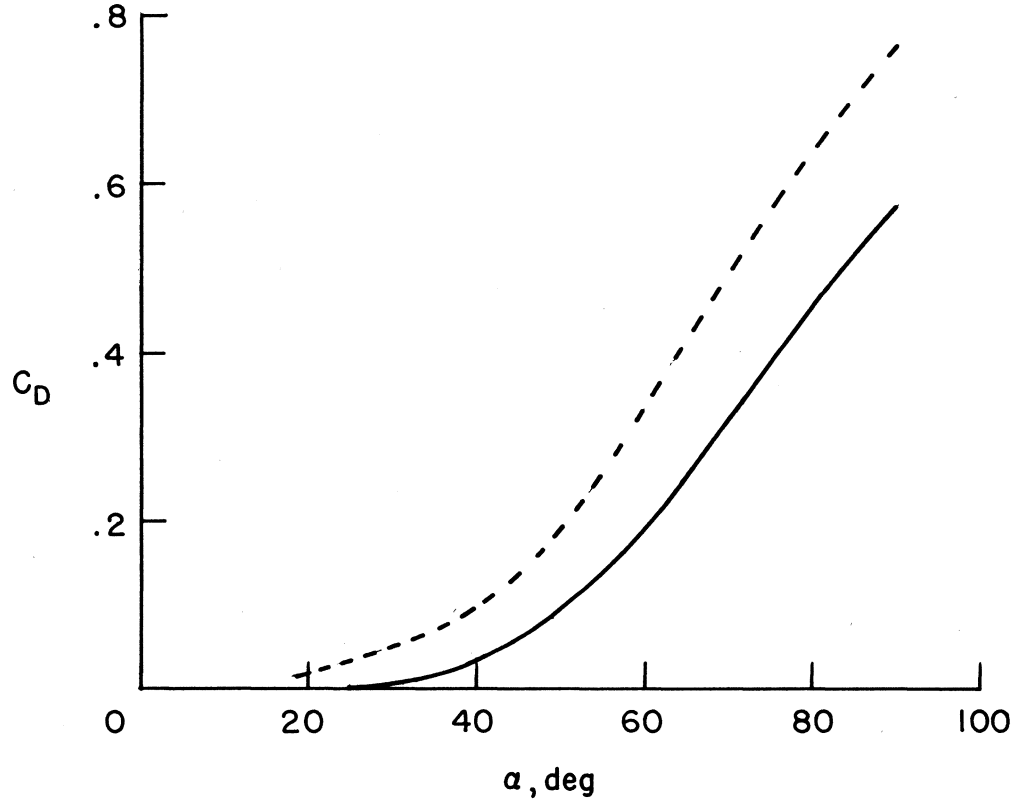

(b) Drag.

Figure 15.- Comparison of lift and drag characteristics of paraglider wing with those of the rigid idealization.

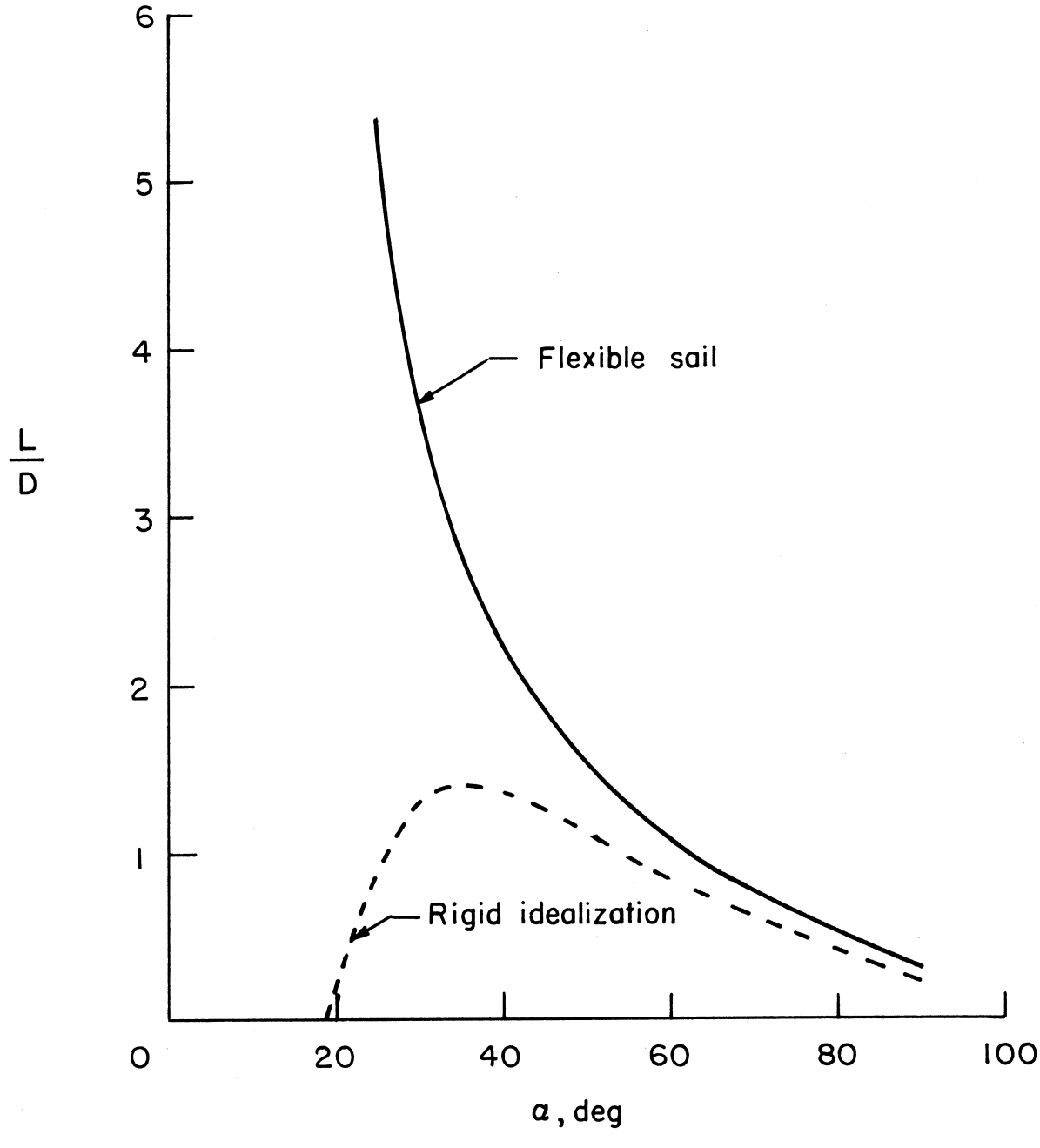

(c) Lift-to-drag ratio.

Figure 15.- Concluded.

the stress resultants in the sail, its dependence on angle of attack is shown in figure 13. The distribution of the stress resultants over the surface of the sail is given in figure 14. The variation of the lift and drag characteristics with angle of attack is given in figure 15.

Effects of changing the dihedral of the wing were also considered. The boundary conditions for this case corresponds to maintaining the value

$$d = 0.4872\ l_K$$

and specifying various values of $\beta(\theta_L)$. These computations were performed for an angle of attack, $\alpha = 35^\circ$. The results are presented in table 2 and in figures 16 through 18. The influence of change of dihedral angle on the deflected shape of the sail is shown in figure 16, and on the variation of pressure coefficient over the surface of the sail in figure 17. Effects of change of dihedral angle on the lift and drag characteristics of the paraglider wing are shown in figure 18.

D. Discussion of Numerical Results

The deflected shape of the flexible sail of the paraglider wing is compared with that for the rigid idealization in figure 11. There is a considerable variance in the deflected shape from that of the rigid idealization at all angles of attack, thus the pressure distribution is different for two wings. The variation of pressure coefficient with angle of attack is shown in figure 12. Figures 11 and 12 show that, as the angle of attack increases, the point of

TABLE 2. FORCE CHARACTERISTICS OF PARAGLIDER WING AT VARIOUS DIHEDRAL ANGLES, $\beta(\theta_L)$

$\beta(\theta_L)$, deg	-15	-10	-5	0	5	10	14.4
$(d\beta/d\theta)_0$	0.98727	0.98702	0.98905	0.99234	0.99574	0.99842	0.99970
$C/q l_K^3$	.01894	.02126	.02153	.01979	.01645	.01190	.007500
F_{Kx_0}/qS	.00304	.00341	.00347	.00322	.00270	.00196	.00124
F_{Ky_0}/qS	.00213	.00241	.00225	.00173	.00107	.000473	.000130
F_{Kz_0}/qS	.0140	.0157	.0160	.0147	.0123	.00888	.00560
F_{Lx_0}/qS	.00778	.00787	.00701	.00548	.00366	.00192	.000760
F_{Ly_0}/qS	-.00633	-.00859	-.0100	-.0103	-.00935	-.00723	-.00475
F_{Lz_0}/qS	.0105	.0114	.0110	.00967	.00760	.00520	.00313
x_{OK}/l_K	.546	.546	.546	.546	.546	.546	.546
y_{OK}/l_K	0	0	0	0	0	0	0
z_{OK}/l_K	-.382	-.382	-.382	-.382	-.382	-.382	-.382
x_{OL}/l_K	.383	.415	.448	.481	.515	.548	.576
y_{OL}/l_K	.264	.293	.310	.315	.310	.293	.368
z_{OL}/l_K	-.478	-.431	-.384	-.337	-.289	-.242	-.201
C_L	.0490	.0542	.0540	.0487	.0397	.0281	.0175
C_D	.0216	.0226	.0210	.0174	.0127	.00777	.00400
L/D	2.26	2.40	2.57	2.80	3.12	3.62	4.37
$\bar{x}_0/l_K$	.476	.491	.506	.520	.534	.547	.557
$\bar{z}_0/l_K$	-.451	-.417	-.384	-.354	-.329	-.313	-.314

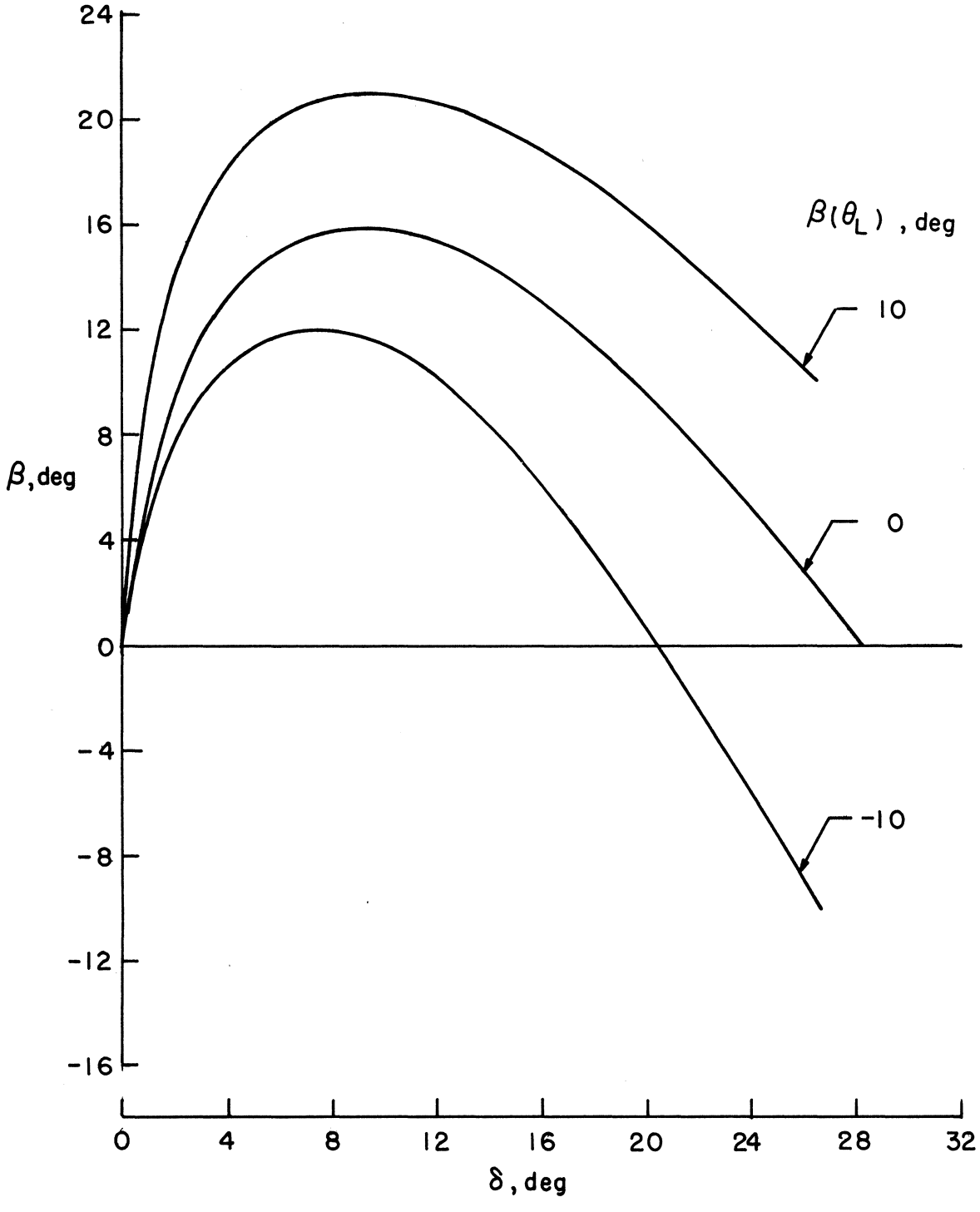

Figure 16.- Variation of deflected shape with dihedral angle $\beta(\theta_L)$. Angle of attack, $\alpha = 35^\circ$.

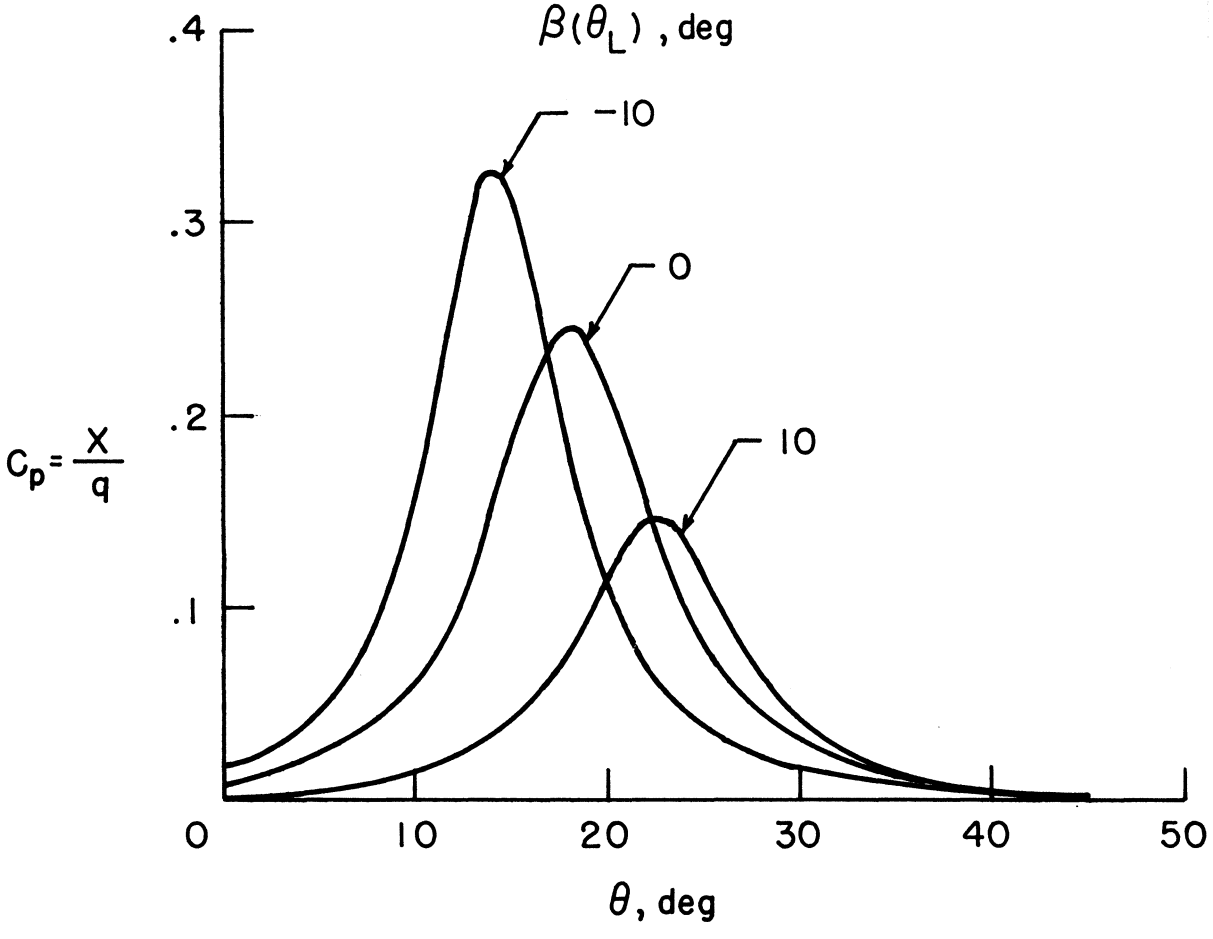

Figure 17.- Variation of pressure coefficient with dihedral angle $\beta(\theta_L)$. Angle of attack, $\alpha = 35^\circ$.

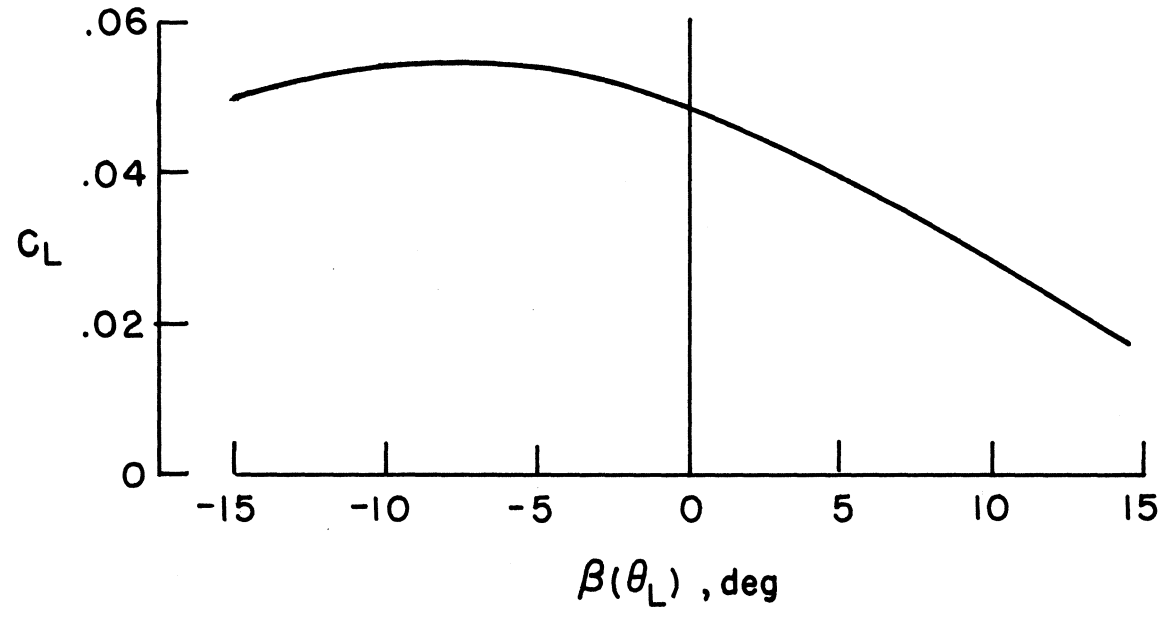

(a) Lift.

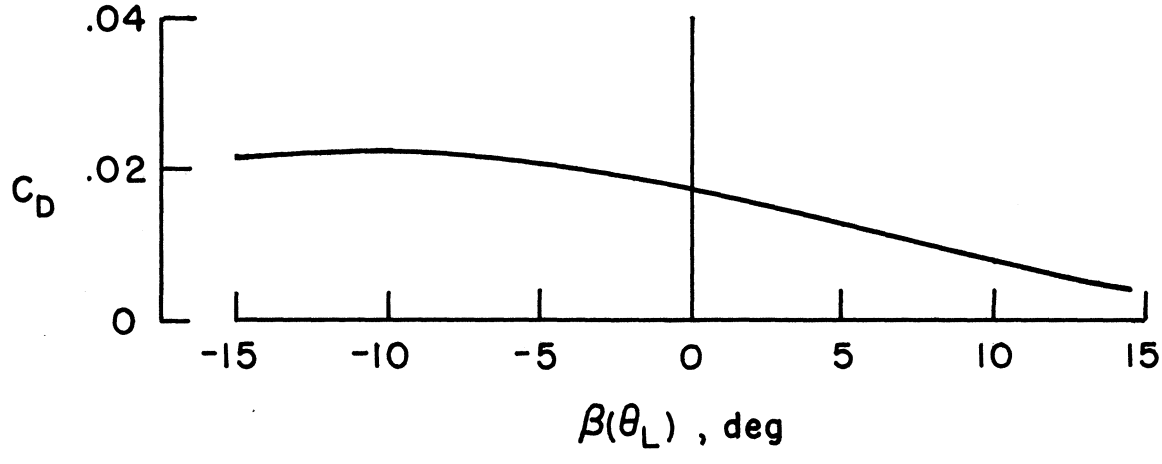

(b) Drag.

Figure 18.- Variation of lift and drag characteristics of paraglider wing with dihedral angle $\beta(\theta_L)$. Angle of attack, $\alpha = 35^\circ$.

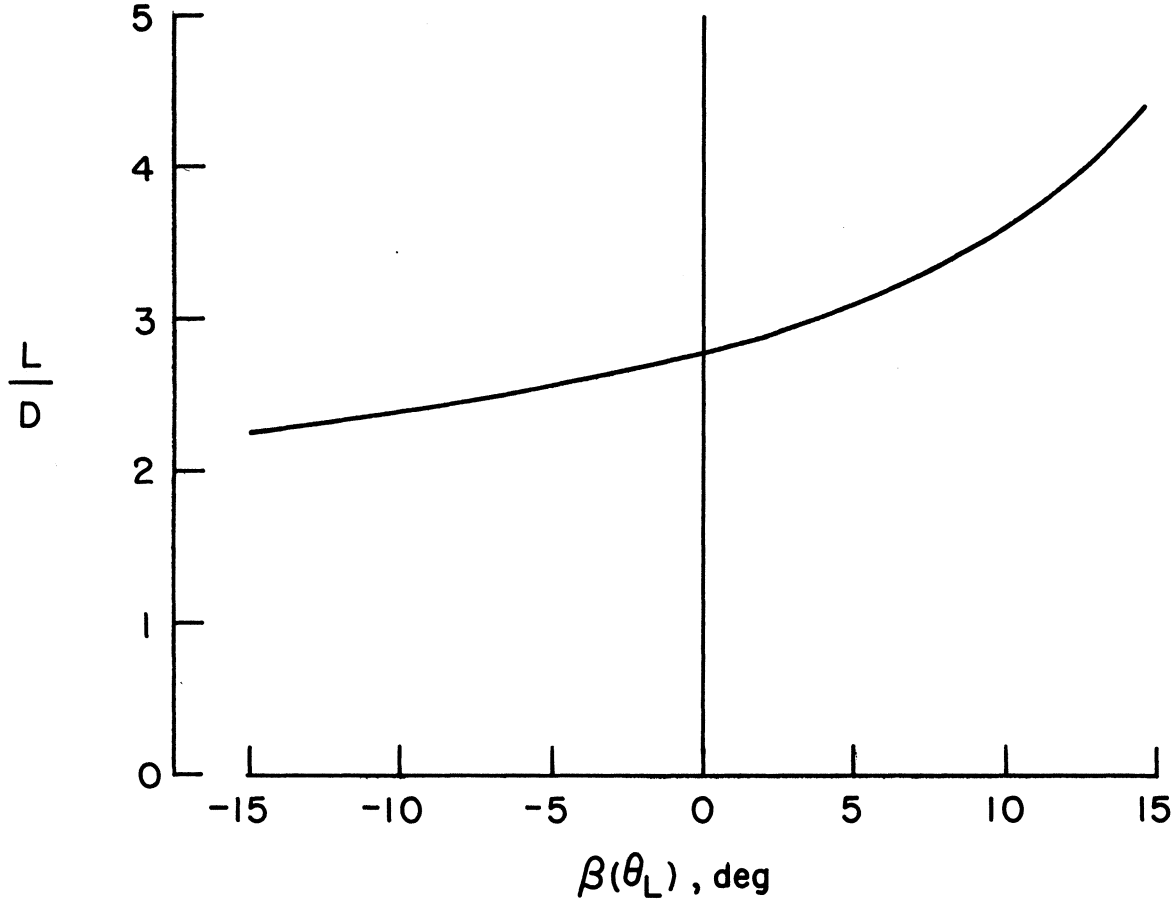

(c) Lift-to-drag ratio.

Figure 18.- Concluded.

maximum deflection and the point of maximum pressure coefficient move outboard from the keel.

The stress resultants, given in figure 14, vary in magnitude with angle of attack through the constant C which can be obtained from figure 13. The magnitudes of the stress resultants, along any radial line from the nose of the wing, are found to be proportional to the distance from the nose. The symmetrical form of the stress resultants is a consequence of having keel and leading-edge booms of equal length. Even though the magnitudes of the stress resultants are dependent on angle of attack, the shapes of the distribution curves are independent of the angle of attack. This result is unexpected since the deflected shape of the sail is different for each angle of attack.

The lift and drag characteristics of the flexible wing are compared with those for the rigid idealization in figure 15. Figures 15(a) and 15(b) show that the arbitrary shape used for the rigid idealization cause an overestimation of the lift and drag forces over the complete range of angle of attack; however, the same trends are apparent for both the rigid and flexible wings. The lift-to-drag ratio, which is a measure of the angle of glide (fig. 1(b)), shows a very significant difference for angles of attack below 50°. Computations were not carried below 25° because of the large amount of computer time needed in order to obtain the deflected shape in this range of angle of attack. This results since in this region small changes in the assumed values of

$C/q l_K^3$ and $(d\beta/d\theta)_0$ produce large changes in the deflected shape. Presumedly, L/D will drop abruptly at some lower value of α. But the results already show that L/D for the flexible sail is more than three times the maximum value of L/D for the rigid idealization.

The resultant forces, applied by the sail to the keel and leading-edge booms, and the location of these forces are given in table 1. These values may be used by the designer for calculating stresses in shroud lines and spreader bars. Stresses in the booms may then be found by analyzing these booms as free-free beams subjected to the self-equilibrating system of loads provided by the sail, shroud lines, and spreader bars.

The influence of change in dihedral angle on the deflected shape of the sail is shown in figure 16. These shapes, yield the distribution of pressure coefficients for figure 17. Figure 17 shows that decreasing dihedral angle (lowering of the leading-edge boom with respect to the keel) tends to move the resultant pressure force inboard toward the keel. Figures 18(a) and 18(b) indicate that the maximum values of lift and drag coefficients are obtained for a dihedral angle of about -8°. The ratio of lift to drag shown in figure 18(c) increases with increase in dihedral angle.

IX. CONCLUDING REMARKS

Equilibrium equations for the sail of the paraglider wing have been derived and integrated, with satisfaction of boundary conditions on stress resultants at the nose of the sail, to yield explicitly the stress resultants in the sail in terms of the pressure on the sail and a parameter that describes the deflected shape of the sail. Certain other important quantities have been expressed in terms of these stress resultants. The resultant forces applied by the sail to the leading-edge booms and keel boom have been obtained by integration of the stress resultants along the edges of the sail and the drag and lift forces have been obtained by considering the streamwise and cross-stream components of the boom forces. The locations of the boom forces and lift and drag forces have also been found. The form of these results is such that they apply for any altitude and speed of the paraglider; they may be used with any appropriate aerodynamic theory. When the appropriate aerodynamic theory for the speed range being considered is used to express the relationship between pressure and deflected shape, the boundary conditions on stress resultants at the trailing edge of the sail yield the criterion for obtaining the deflected shape of the sail. The general formulas may then be applied to calculate the stress resultants, lift, and drag.

In order to show an application of the analysis, the equations have been specialized for Newtonian impact theory, which has been used in various analyses to express the aerodynamic pressure - deflected shape relationship for the hypersonic speed range. Numerical results have been obtained and have been compared with the

results for a rigid idealization of the paraglider wing. The comparison showed that the deflected shape of the flexible paraglider wing differed considerably from the assumed shape of the rigid wing over the complete range of angles of attack. This difference in shape resulted in different pressure distributions over the surface of the sail. Consequently, the lift and drag coefficients and, especially the lift-to-drag ratio, for the flexible wing were significantly different from the values for the rigid wing. Thus use of rigid idealizations in wind-tunnel investigations to draw conclusions as to the aerodynamic characteristics of the paraglider - especially the lift-to-drag ratio - may be misleading.

The calculated stress resultants and boom forces provide a basis for design of sails, booms, shroud lines, and spreader bars for a paraglider for hypersonic flight.

The analysis was performed for a sail with a straight trailing edge. Use of a different trailing-edge contour would have altered the trailing-edge boundary conditions on the stress resultants. Since these trailing-edge boundary conditions, upon the assumption of an aerodynamic theory for a pressure-shape relationship, yield the criterion for defining the deflected shape, the trailing-edge contour could be an important consideration in the design of a paraglider wing.

X. SUMMARY

Equilibrium equations for the sail of a paraglider wing are derived. Upon integration of these equations and satisfaction of the boundary conditions at the nose of the sail, expressions are found for the stress resultants in terms of the pressure on the sail and a parameter that describes the deflected shape of the sail. The lift and drag forces are obtained by integration of the stress resultants along the keel and leading-edge boundaries of the sail. The boundary conditions on stress resultants at the trailing edge of the sail, upon substitution of an aerodynamic relation between pressure and deflected shape, yield a criterion for obtaining the deflected shape. Numerical results were obtained for Newtonian impact aerodynamic theory and were compared with published results obtained for a rigid idealization of the paraglider wing. It was found that the assumed rigid idealization did not approximate the shape of a flexible wing well and led to significant errors in the lift and drag forces and the lift-to-drag ratio. The new calculations provide a basis for design of paragliders for hypersonic flight.

XI. ACKNOWLEDGMENTS

Thanks are due to the National Aeronautics and Space Administration for permitting this work to be carried out as part of the author's daily work at the NASA Langley Research Center. The author would like to express his thanks to Dr. Robert W. Leonard of the NASA Langley Research Center for suggesting the problem and to Professor Daniel Frederick of the Virginia Polytechnic Institute for his suggestions and encouragement.

XII. BIBLIOGRAPHY

1. Rogallo, Francis M., Lowry, John G., Croom, Delwin R., and Taylor, Robert T.: Preliminary Investigation of a Paraglider. NASA TN D-443, August 1960.

2. Naeseth, Rodger L.: An Exploratory Study of a Parawing as a High-Lift Device for Aircraft. NASA TN D-629, Nov. 1960.

3. Hewes, Donald E.: Free-Flight Investigation of Radio-Controlled Models With Parawings. NASA TN D-927, Sept. 1961.

4. Taylor, Robert T.: Wind-Tunnel Investigation of Paraglider Models at Supersonic Speeds. NASA TN D-985, Nov. 1961.

5. Fournier, Paul G., and Bell, B. Ann: Low Subsonic Pressure Distributions on Three Rigid Wings Simulating Paragliders With Varied Canopy Curvatures and Leading-Edge Sweep. NASA TN D-983, Nov. 1961.

6. Fournier, Paul G., and Bell, B. Ann: Transonic Pressure Distributions on Three Rigid Wings Simulating Paragliders With Varied Canopy Curvature and Leading-Edge Sweep. NASA TN D-1009, Jan. 1962.

7. Penland, Jim A.: A Study of the Aerodynamic Characteristics of a Fixed Geometry Paraglider Configuration and Three Canopies With Simulated Variable Canopy Inflation at a Mach Number of 6.6 NASA TN D-1022, March 1962.

8. Johnson, Joseph L., Jr., and Hassell, James L., Jr.: Summary of Results Obtained in Full-Scale Tunnel Investigation of the Ryan Flex-Wing Airplane. NASA TM SX-727, June 1962.

9. Leonard, Robert W.: Nonlinear First Approximation ThinsShell and Membrane Theory. Ph. D. Thesis, Virginia Polytechnic Institute, Blacksburg, 1961.

10. Truitt, Robert Wesley: Hypersonic Aerodynamics. The Roland Press, New York, 1959.

11. Hayes, W. D., and Probstein, R. F.: Hypersonic Flow Theory. Academic Press, New York, 1959.

The vita has been removed from the scanned document

STRESS AND SHAPE ANALYSIS OF A PARAGLIDER WING

By

Robert W. Fralich

ABSTRACT

The paraglider wing consists of leading-edge booms and a keel boom joined together at the nose and a flexible sail whose surface carries the aerodynamic pressure loading. The payload is suspended beneath the wing by cables which are used to control the wing. Adjusting the length of these cables controls the glide path of the wing by shifting the position of the payload with respect to the wing.

The deflected shape of the sail depends on the pressure distribution over the sail; the pressure distribution in turn depends aerodynamically on the deflected shape of the sail. It is the purpose of this thesis to derive the equilibrium equations for the sail and to integrate these equations to find expressions for the stress resultants in terms of the pressure on the sail and the deflected shape of the sail. By integration of these expressions for stress resultants, along the edges of the sail, the resultant forces applied by the sail to the leading-edge booms and keel boom are found. Then, by considering the streamwise components and the components normal to the stream of the boom forces, the drag and lift forces are obtained. These expressions for the lift and drag forces, and for the boom forces, are given in terms of the boundary

value of the stress resultants and can be applied for any aerodynamic theory appropriate to the speed range being considered. When the appropriate aerodynamic relationship, between pressure and deflected shape, is substituted into the boundary conditions for stress resultant at the trailing edge of the sail, the criterion for determining the deflected shape is obtained. Once the deflected shape is known all the other quantities can be determined.

In order to show an application of the analysis, the equations were specialized for Newtonian impact theory. This theory yields a simple pressure-deflected shape relationship. This aerodynamic theory, which has found applications for hypersonic speeds, has been employed since it shows the application of the method in a simple manner. In addition, it has been applied previously for a rigid idealization of a paraglider wing and thus provides a ready means for comparison. Hence numerical results can be used to test the accuracy of the rigid idealization. These results showed that the deflected shape of the flexible paraglider wing differed considerably from the conical shape of the rigid wing over the complete range of angle of attack. The differences in shape result in different pressure distributions over the surface of the wing and as a result the lift and drag coefficients, and especially the lift-to-drag ratio, for the flexible wing were significantly different from the values for the rigid wing. The boom forces and the distribution of stress resultants over the surface of the sail were obtained. The stress resultants along radial lines were found to be proportional to the distance from the nose of the wing. The calculated stress resultants

and boom forces provide a basis for design of sails, booms, shroud lines, and spreader bars for a paraglider for hypersonic flight.

Effects of dihedral angle (raising or lowering of the leading-edge booms relative to the keel) were also considered. The pressure distributions, the lift and drag coefficients, and the ratio of lift to drag were found for several dihedral angles at a given angle of attack.